EUROfusion

Materials Simulation Programme in the EU

S.L. Dudarev, G. Apostolopoulos, G. Aiello, M.-F. Barthe, M. Boleininger, M.J. Caturla, C.-C. Fu, A. Feichtmayer, T. Jourdan, K. Iroc, E. Gaganidze, A. Gentils, F. Granberg, M. Klimenkov, A. Laukkanen, A. London, P.-W. Ma, M.-C. Marinica, S. Markelj, D.R. Mason, K. Mergia, K. Nordlund, P. Olsson, C.J. Ortiz, G. Pintsuk, L. Reali, J. Riesch, C. Robertson, A.E. Sand, H.C. Schneider, F. Soisson, T. Schwarz-Selinger, T.D. Swinburne, T. Tadić, D. Terentyev, L. Ventelon, J.S. Wróbel, Q. Yuan, M. Zibrov

UK Atomic Energy Authority

This work has been carried out within the framework of the EUROfusion Consortium, funded by the European Union via the Euratom Research and Training Programme (Grant Agreement No 101052200 — EUROfusion). Views and opinions expressed are however those of the author(s) only and do not necessarily reflect those of the European Union or the European Commission. Neither the European Union nor the European Commission can be held responsible for them.

Exposure of structural materials to neutrons

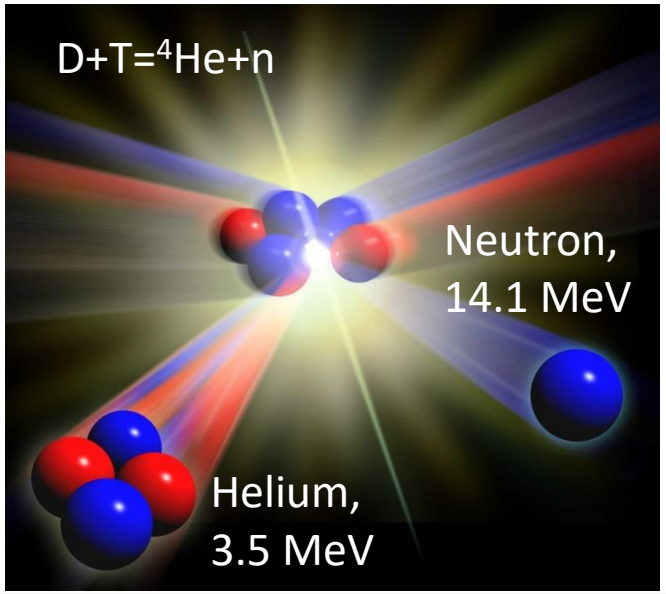

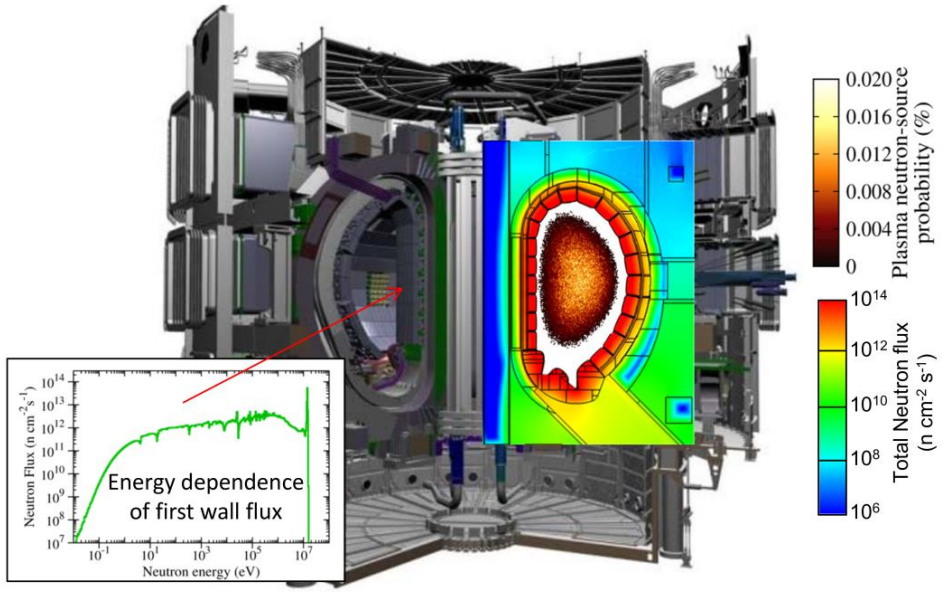

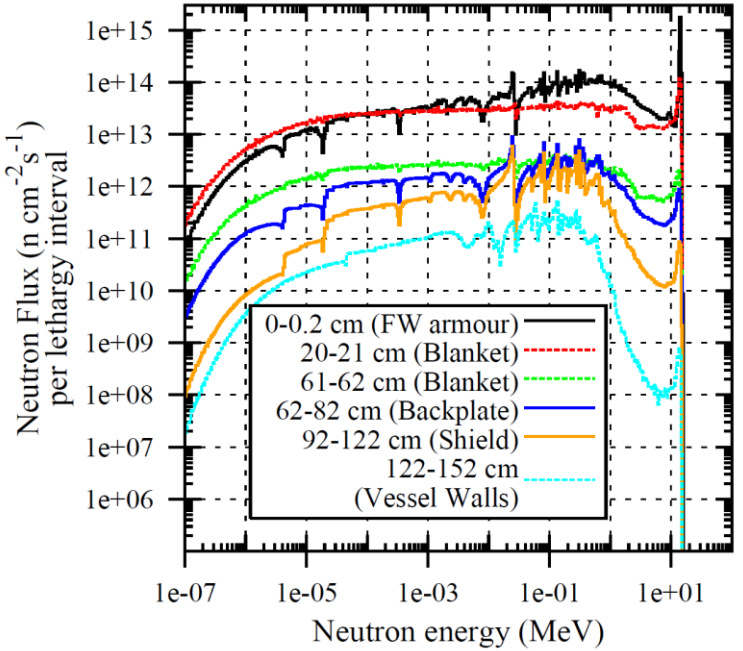

M.R. Gilbert, J.-Ch. Sublet, Nucl. Fusion **51** (2011) 043005

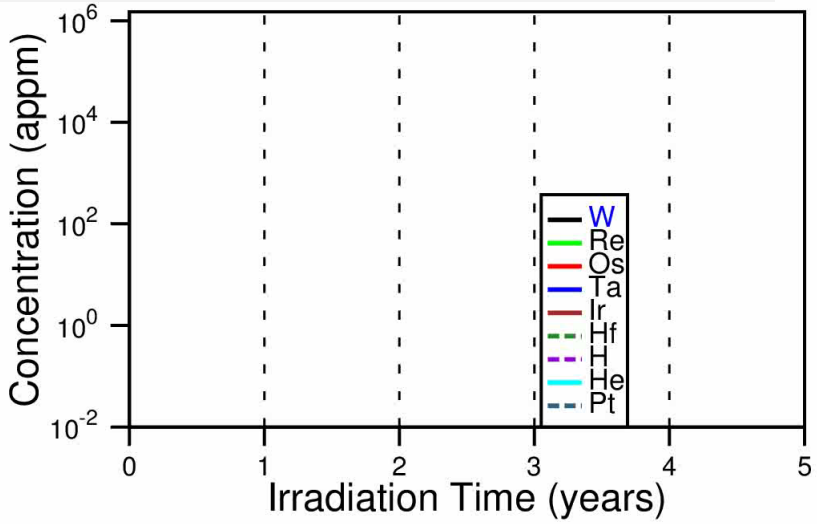

Two fundamental effects of neutron exposure:

- Transmutations
- Formation of microscopic radiation defects

Transmutations change chemical composition. Radiation defects change microstructure.

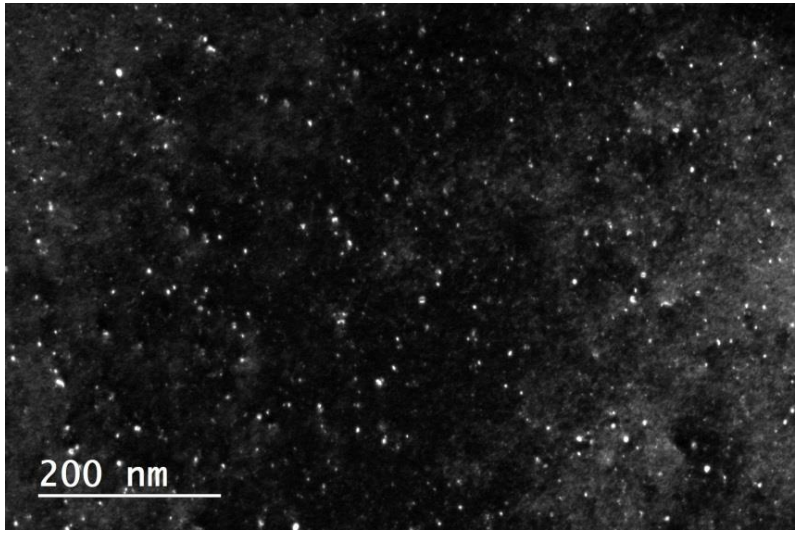

X. Yi *et al.*, EPL **110** (2015) 36001

Fundamentals of neutron exposure

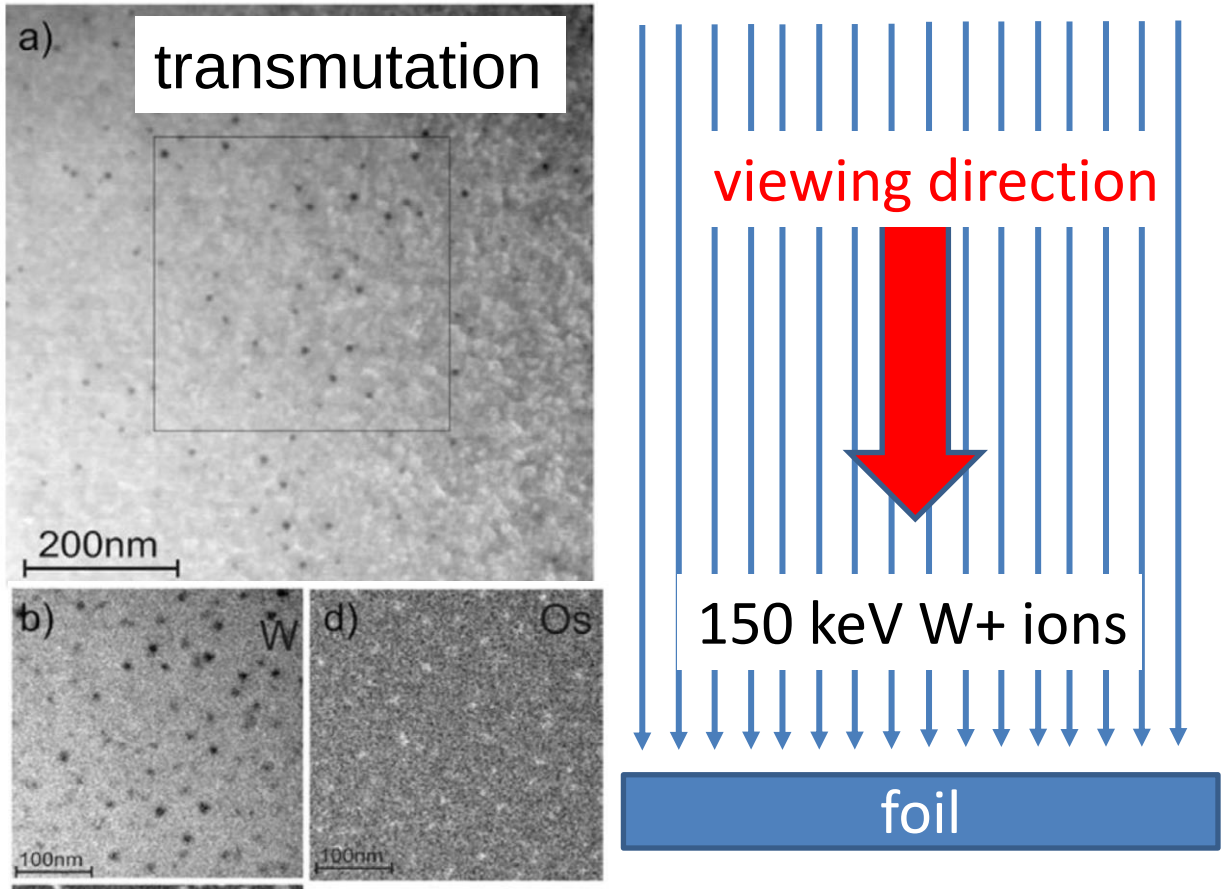

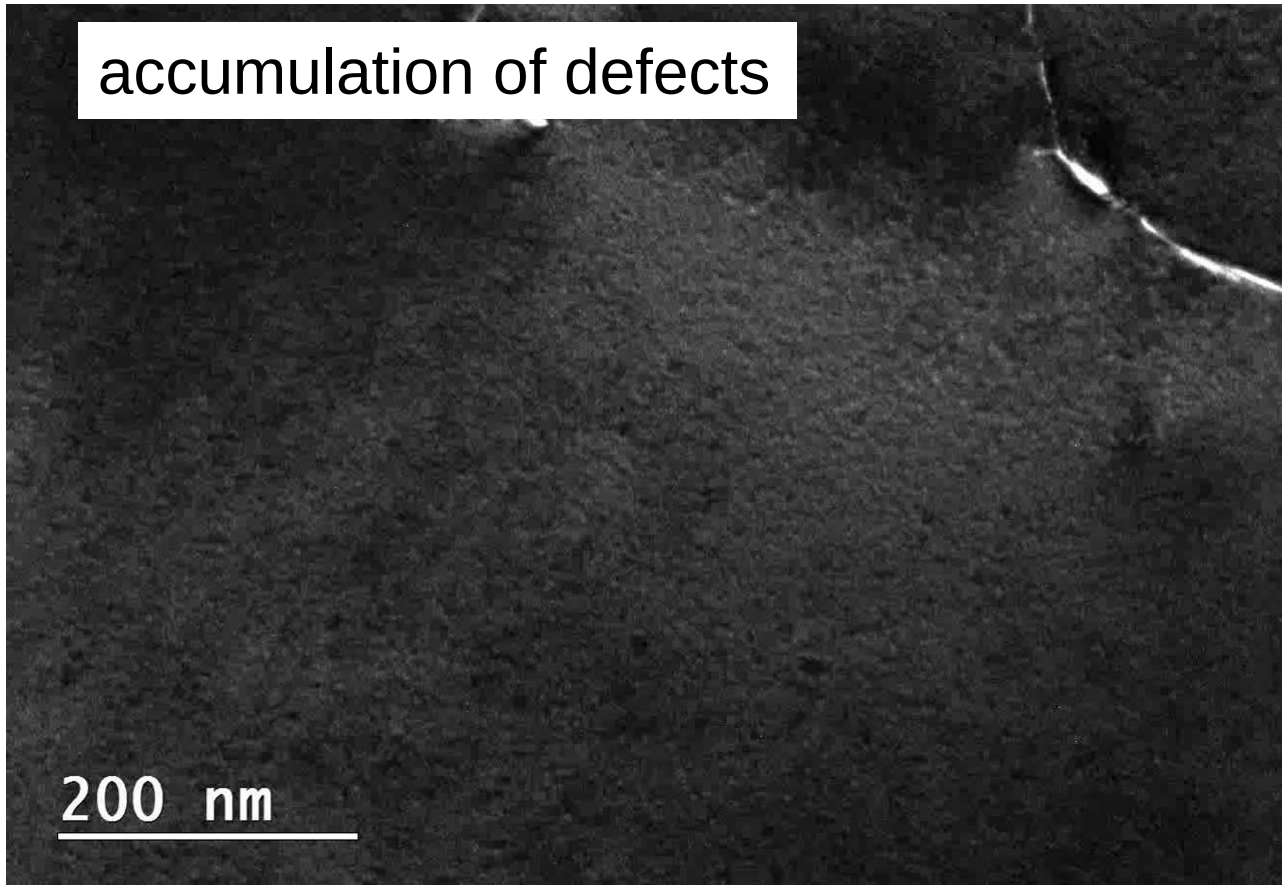

Left: Elemental mapping of tungsten exposed to 1.6 dpa of fission neutron irradiation at 900°C. HAADF image (a), and elemental maps of W (b), Re (c) and Os (d).
Right: *In situ* transmission electron microscope observation of radiation defects in pure tungsten bombarded by 150 keV W+ ions at 30K. Events start overlapping at ~0.1 dpa.

M. Klimenkov *et al.*, Nuclear Materials and Energy **9** (2016) 480; X. Yi *et al.*, EPL **110** (2015) 36001

Interaction of neutrons with atomic nuclei: effect of atomic weight

Material	DEMO			HFR		
	total [W/g]	photon [W/g]	ratio	total [W/g]	photon [W/g]	ratio
W	2.73	2.65	97.1%	10.48	10.36	98.8%
Zr	1.06	0.835	78.8%	0.613	0.343	56.0%
Cu	1.79	1.28	71.5%	3.08	2.75	89.3%
Fe	1.68	1.19	70.8%	2.00	1.63	81.5%
Be	3.65	2.89×10^{-3}	0.08%	2.15	8.40×10^{-7}	0.00004%

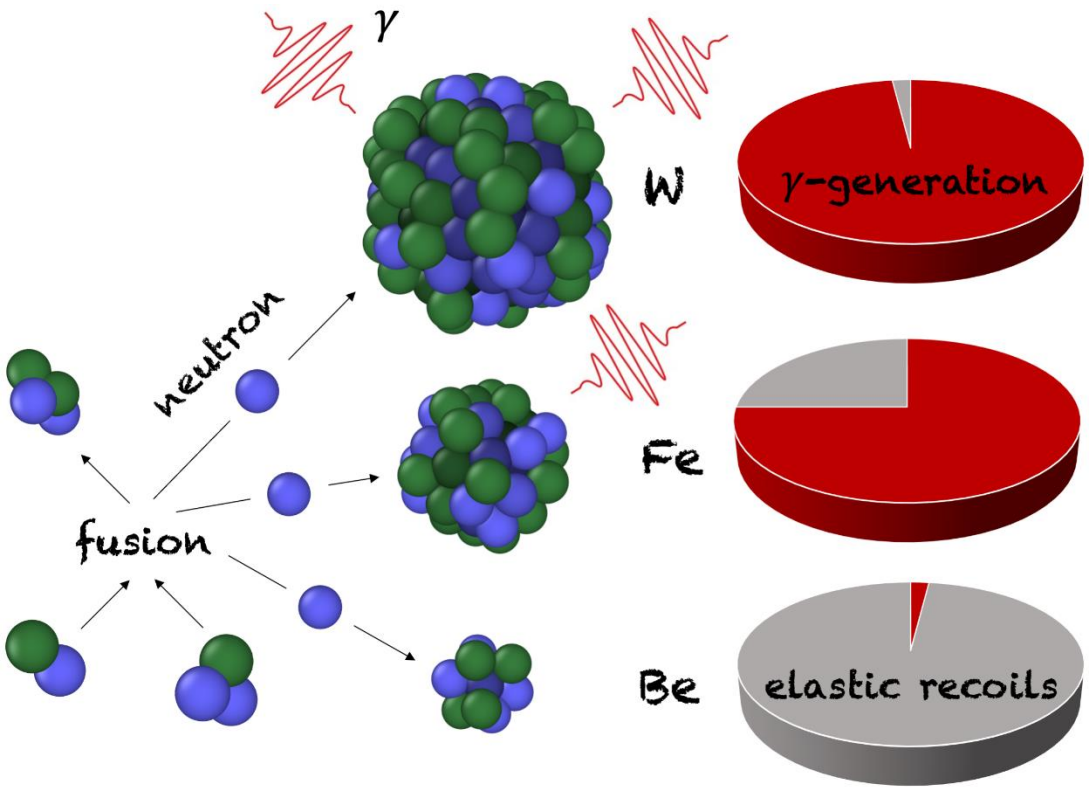

In medium and heavy elements, including Fe, Cu and W, the energy of neutrons is ***not*** deposited as recoils, but is mostly released as electromagnetic γ-radiation. Internal energy levels of large nuclei relax by radiative transitions, generating γ-quanta with MeV energies.

In tungsten, only 1% of neutron energy is deposited as elastic atomic recoils; hence relatively few defects are produced by high energy neutrons. Dissimilar to ion irradiation. Energy deposition is *non-local*.

L. Reali *et al.*, PRX Energy **2** (2023) 023008; JNM **585** (2023) 154584

Fundamentals of neutron exposure

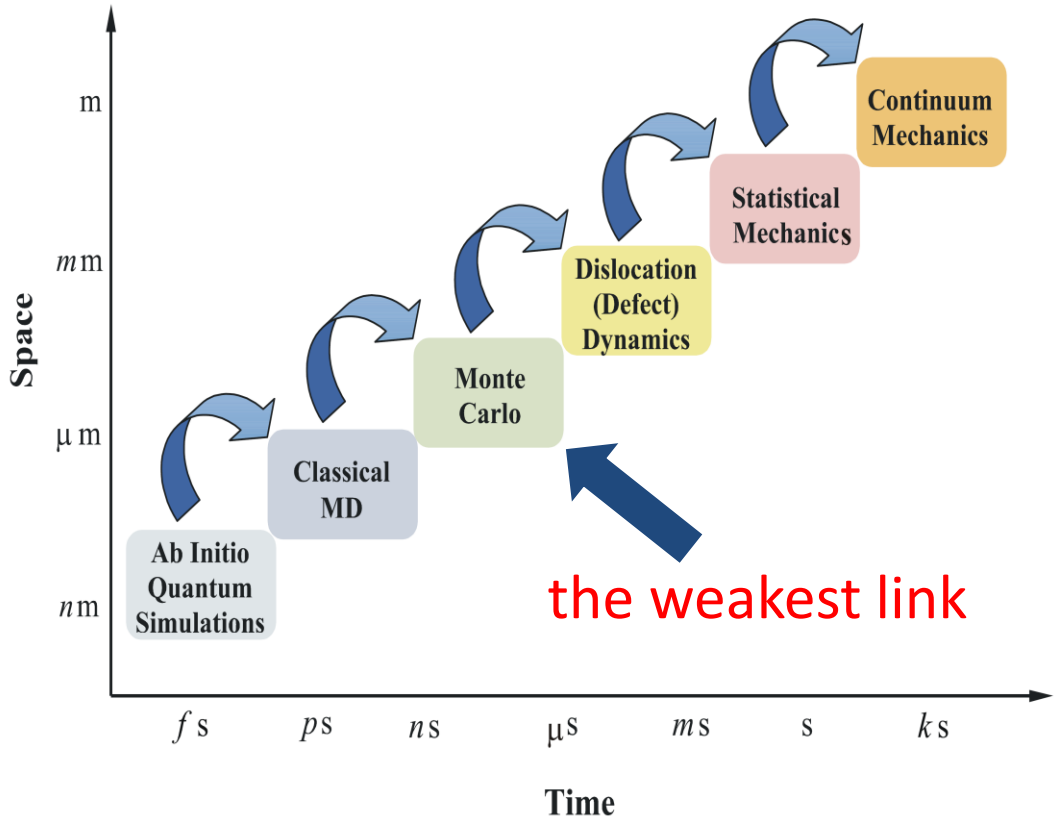

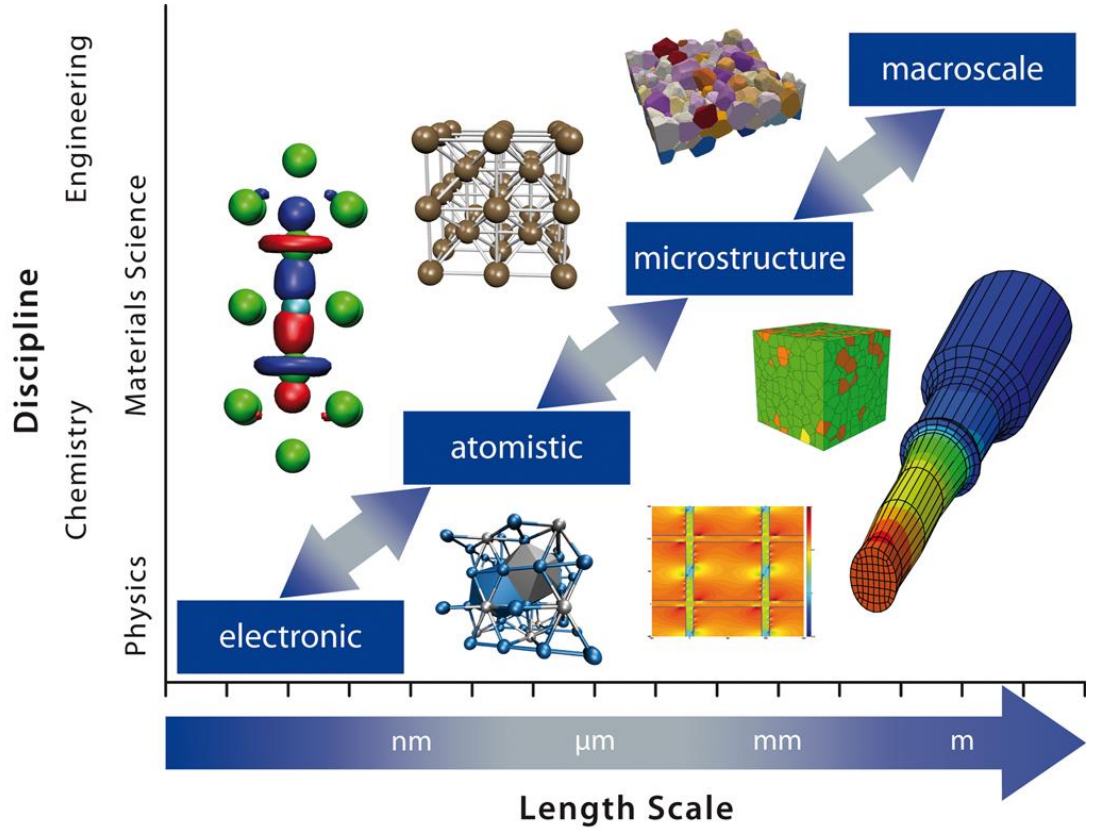

Multiscale modelling concept assumes that if elementary defects are known, macroscopic quantities can be evaluated. This is in general not correct since:

- Not only the individual defects matter, but the collective behaviour of ensembles of defects
- The above hierarchy does not offer a rule for computing macroscopic stress and strain

What are the defects?

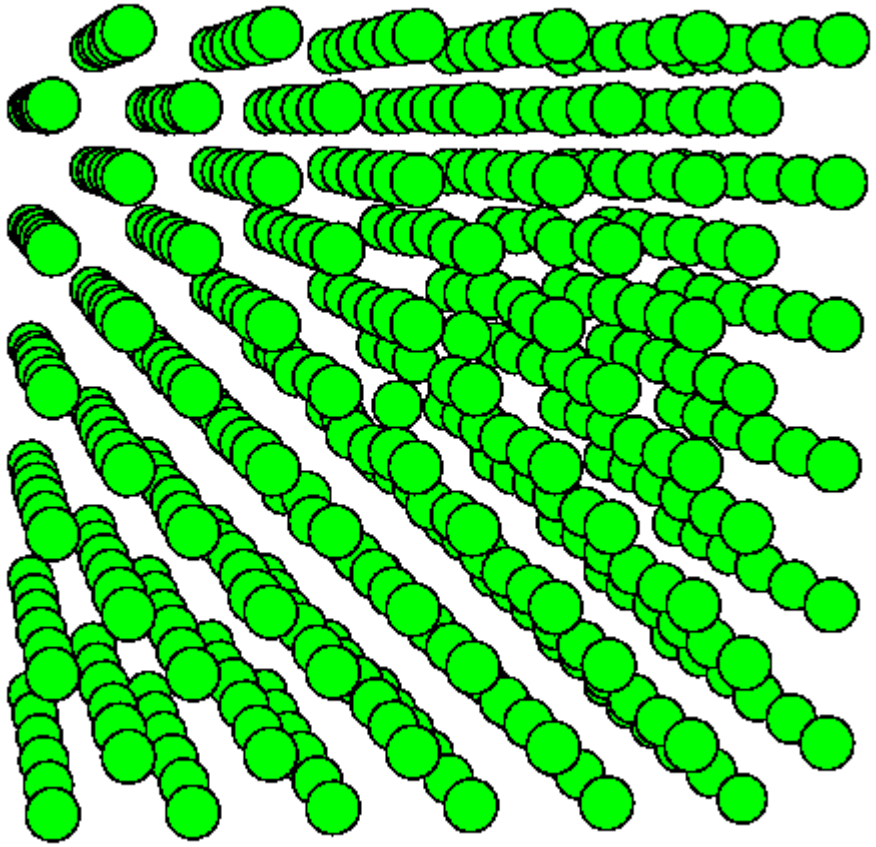

Body-centred cubic crystal lattice of iron, containing ~500 atoms. Defects form if we add or remove atoms from this structure, and let all the atoms relax to the new equilibrium.

By adding one atom, we form a self-interstitial atom (SIA) defect.

By removing an atom, we form a vacancy defect.

The structure of a one-extra-atom (self-interstitial) defect in iron

What are the defects?

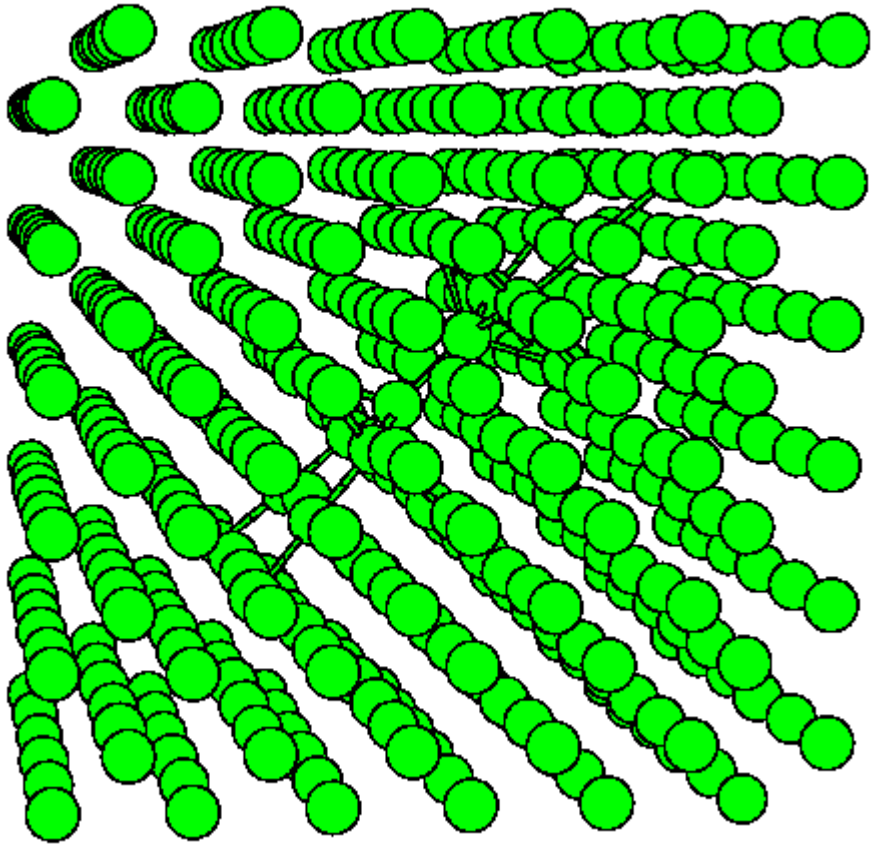

Body-centred cubic crystal lattice of iron, containing ~500 atoms. Defects form if we add or remove atoms from this structure, and let all the atoms relax to the new equilibrium.

By adding one atom, we form a self-interstitial atom (SIA) defect.

By removing an atom, we form a vacancy defect.

The structure of a one-extra-atom (self-interstitial) defect in iron

What are the defects?

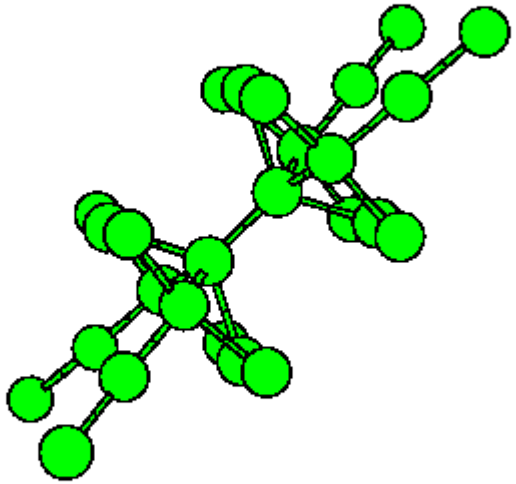

Body-centred cubic crystal lattice of iron, containing ~500 atoms. Defects form if we add or remove atoms from this structure, and let all the atoms relax to the new equilibrium.

By adding one atom, we form a self-interstitial atom (SIA) defect.

By removing an atom, we form a vacancy defect.

The structure of a one-extra-atom (self-interstitial) defect in iron

Thermal migration of self-interstitial defects

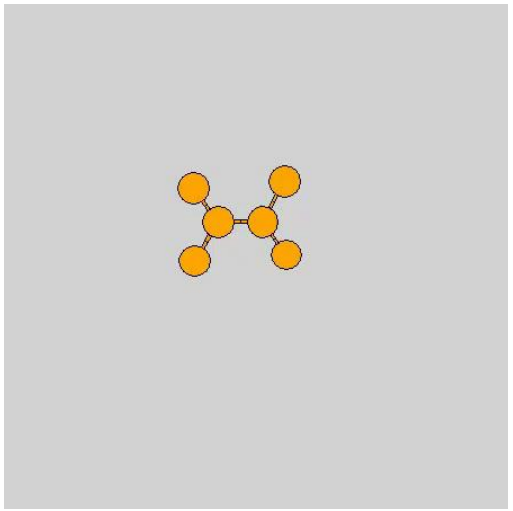

300K

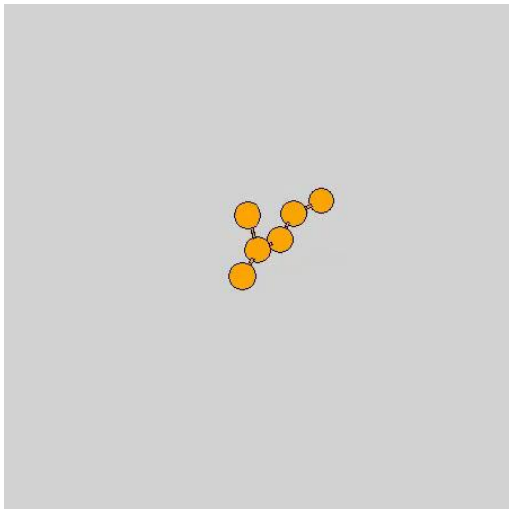

500K

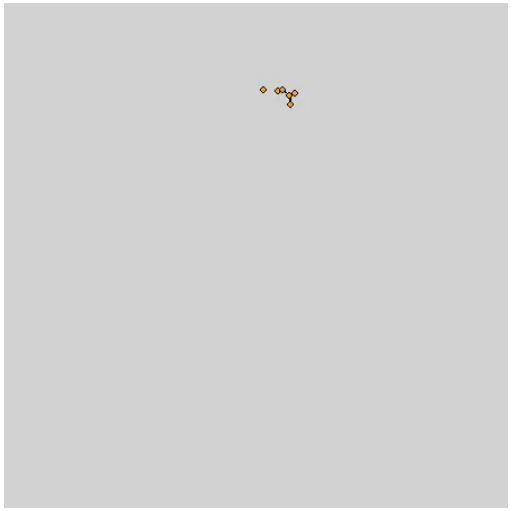

800K

Spontaneous thermal migration of radiation defects is a factor driving microstructural evolution.
Has been extensively studied by atomistic simulations and transmission electron microscopy.

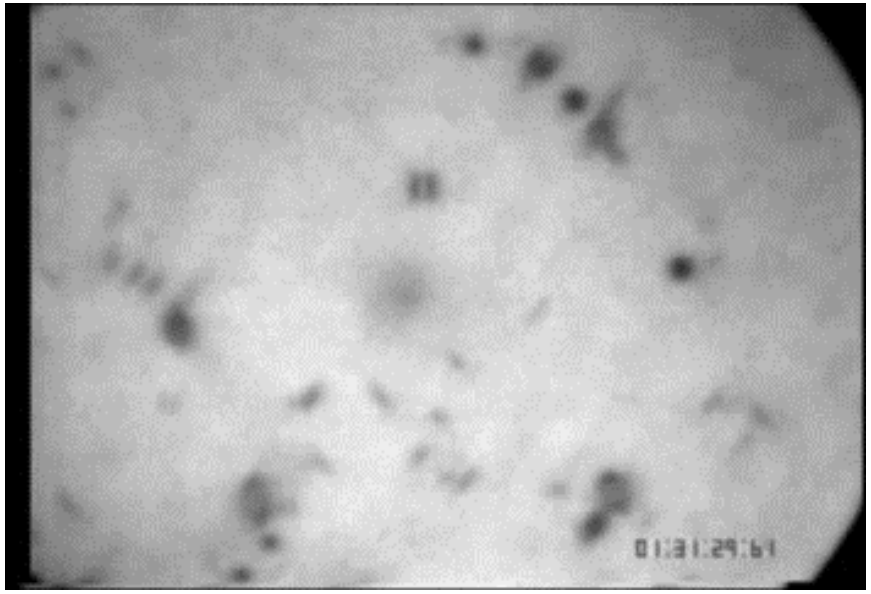

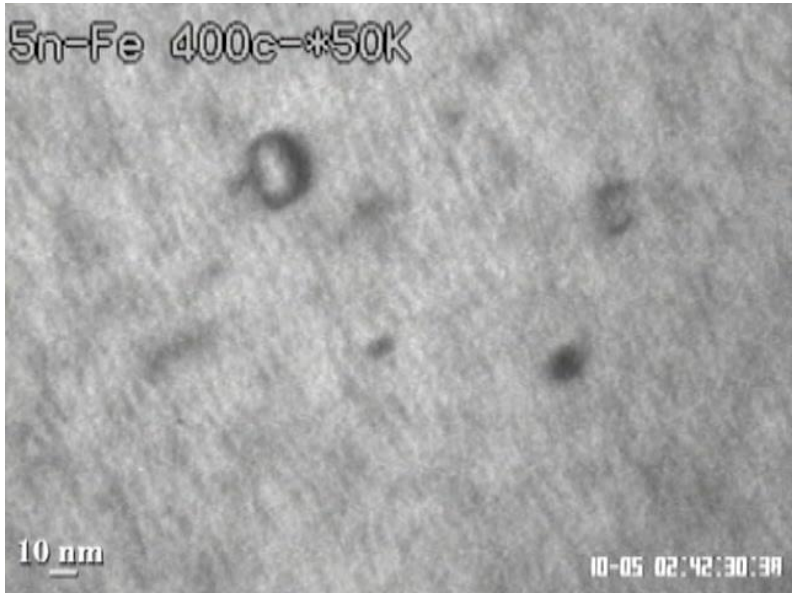

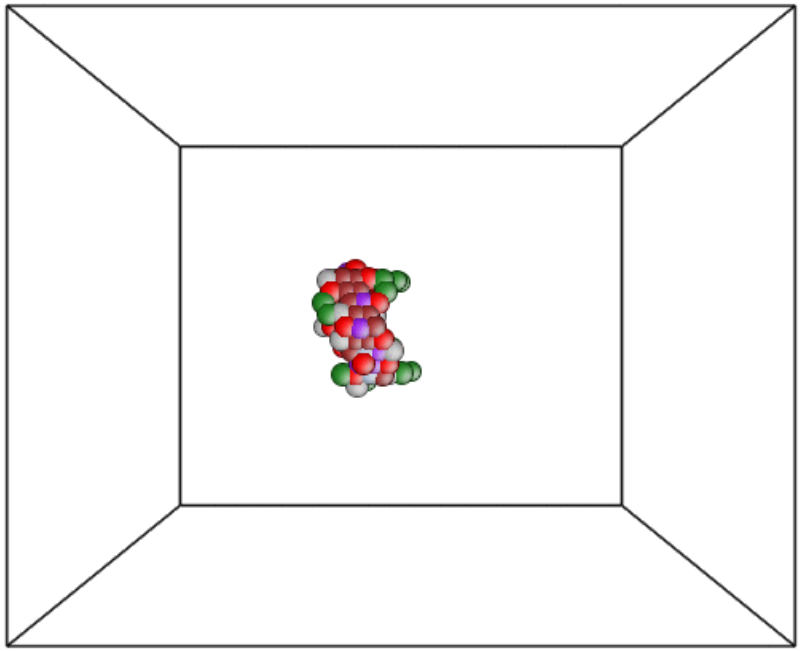

K. Arakawa *et al.*, Science **318** (2007) 956

New algorithms for defect production at high dose

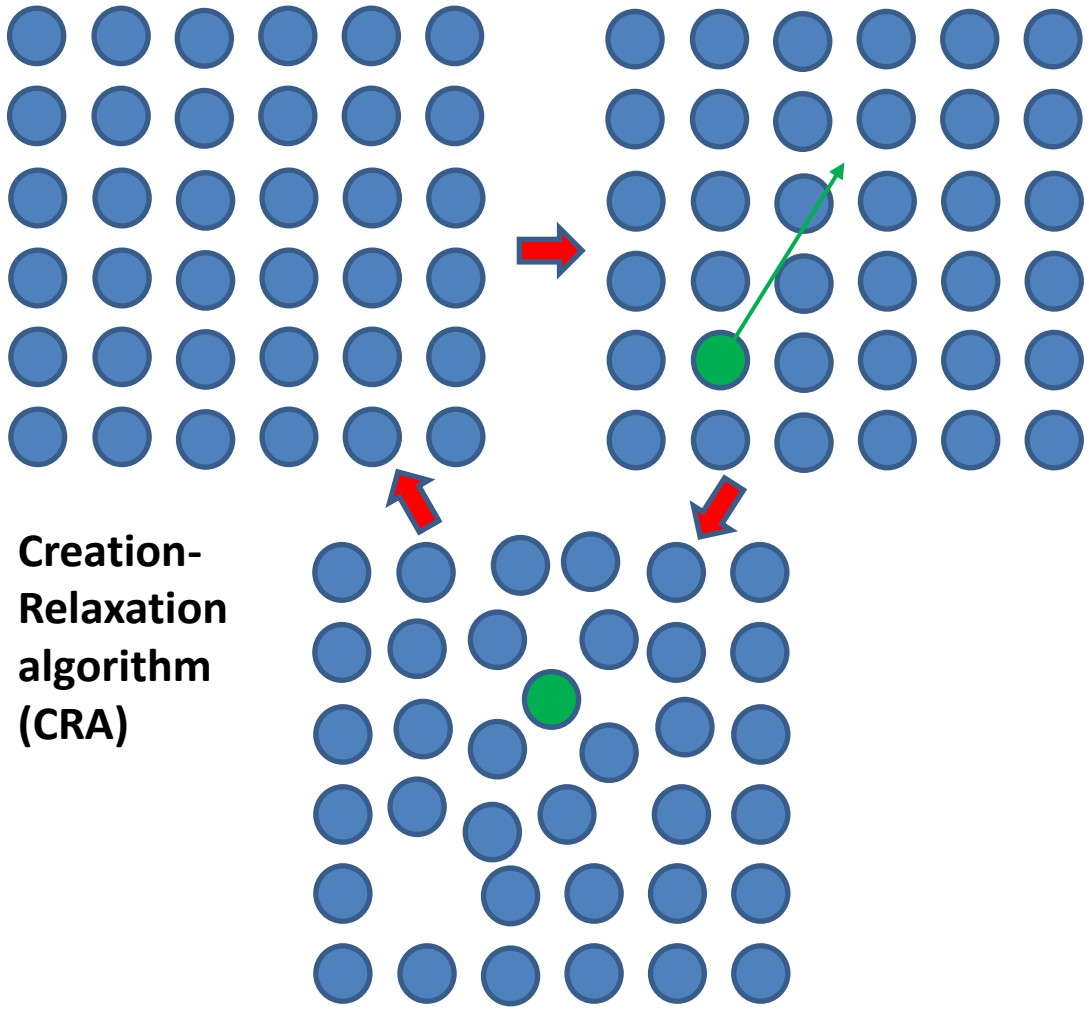

Creation-Relaxation algorithm (CRA)

$$\frac{\text{number of steps}}{\text{number of atoms}} = \text{dpa } (\textit{canonical})$$

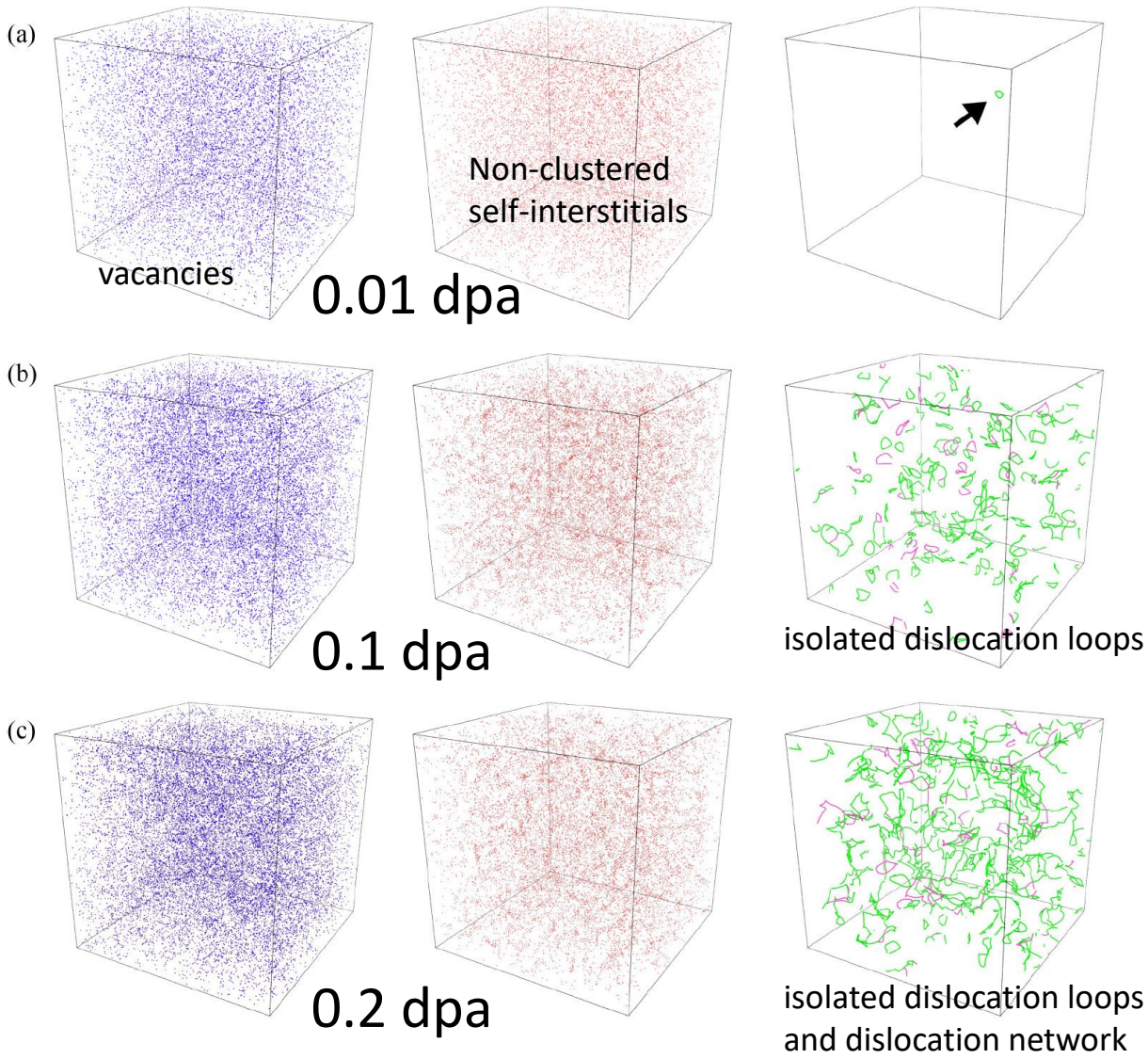

P.M. Derlet and S.L. Dudarev, Phys. Rev. Materials **4** (2020) 023605

Experimental observation of defect production at high dose

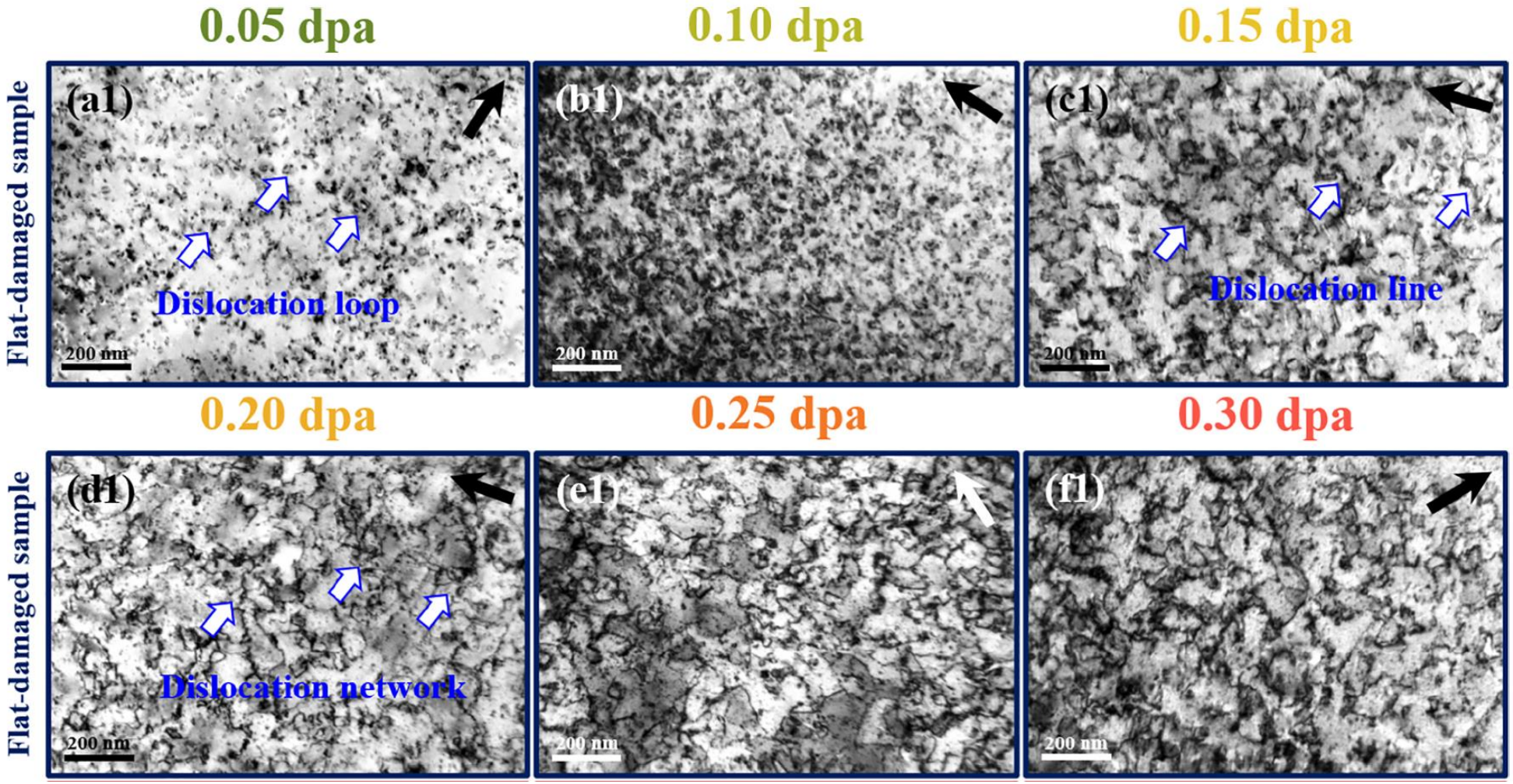

Transmission electron microscope examination of ion-irradiated tungsten confirms the predicted pattern of evolution, from individual dislocation loops at a low dose to a complex network of dislocations at a high dose.
Vacancies not observed.

S. Wang *et al.*, Acta Materialia **244** (2023) 118578

Ab initio models for high dose defect microstructures

Can be readily applied to complex alloys: major drawback of interatomic potentials is the lack of fidelity for alloys

DFT simulation cell size: 1024 atoms; bcc FE, bcc FeCr; spin-polarised, multiple sampling; conjugate gradient with adaptive time step

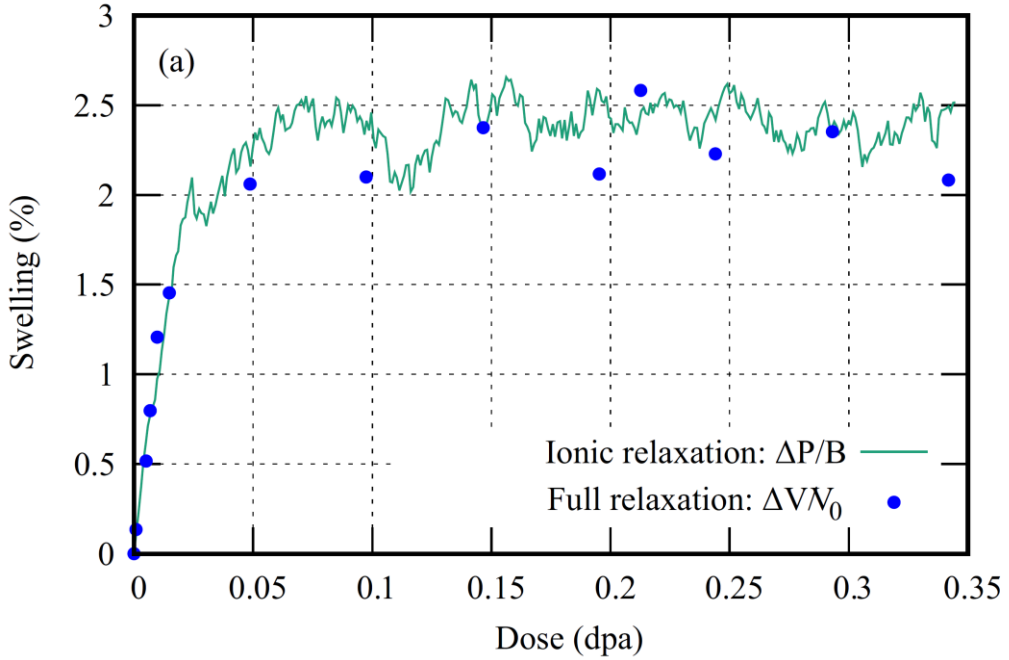

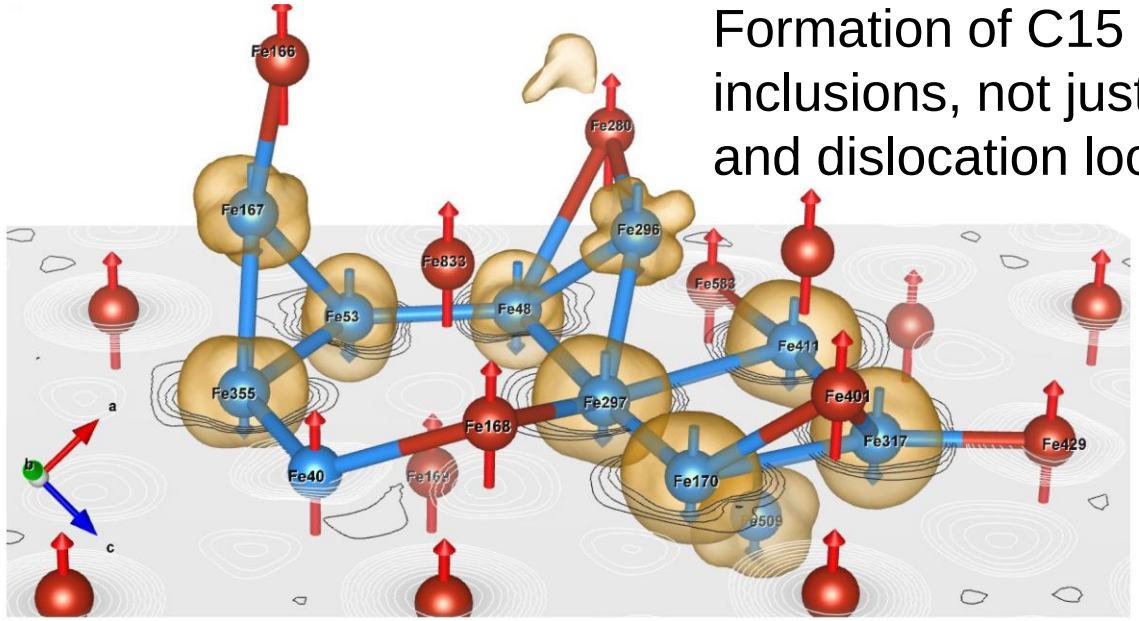

Formation of C15 phase inclusions, not just vacancies and dislocation loops

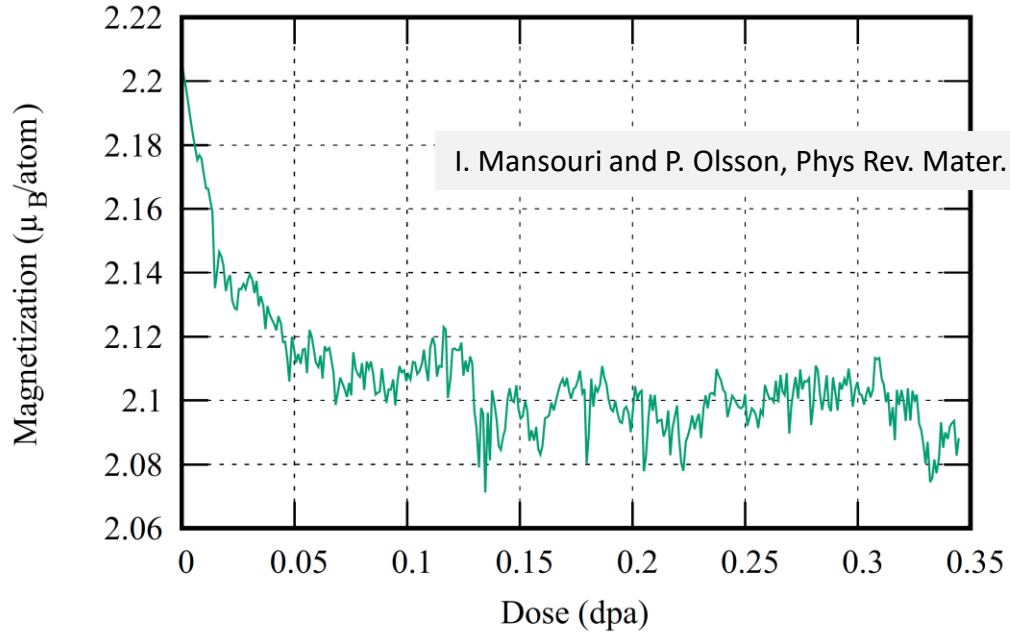

I. Mansouri and P. Olsson, Phys Rev. Mater. **7** (2023) 123604

Predicting high-temperature properties of tungsten from *ab initio* data

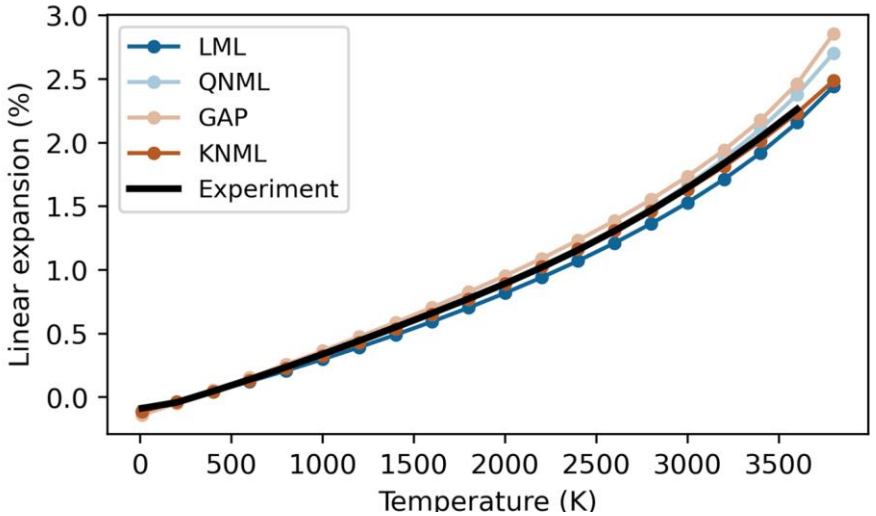

$$\frac{C_{11}^{T}(T)}{C_{11}^{T}(T_{\mathrm{Debye}})} = -3.018 \times 10^{-13} T^{3} - 2.209 \times 10^{-8} T^{2} - 6.875 \times 10^{-5} T + 1.029,$$

$$\frac{C'^{T}(T)}{C'^{T}(T_{\mathrm{Debye}})} = 5.800 \times 10^{-12} T^{3} - 5.166 \times 10^{-8} T^{2} - 1.103 \times 10^{-4} T + 1.054,$$

$$\frac{C_{44}^{T}(T)}{C_{44}^{T}(T_{\mathrm{Debye}})} = -2.592 \times 10^{-12} T^{3} - 1.343 \times 10^{-10} T^{2} - 6.616 \times 10^{-5} T + 1.026.$$

A. Zhong, C. Lapointe, A.M. Goryaeva , J. Baima, M. Athènes , M.-C. Marinica, Phys. Rev. Mater. **7** (2023) 023802

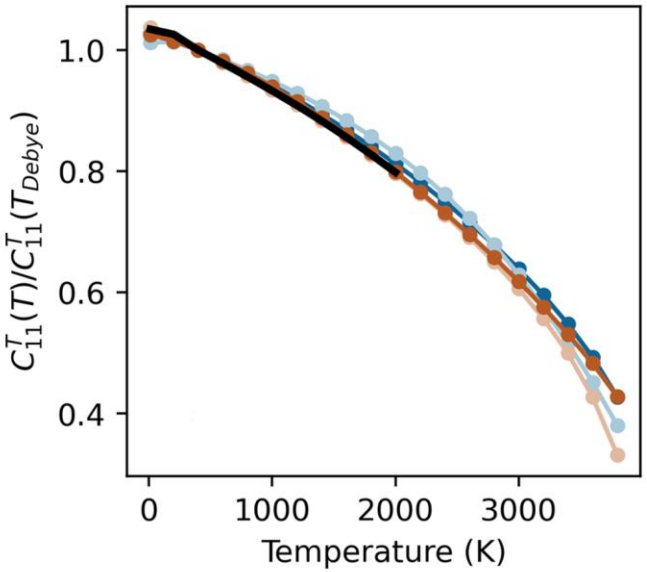

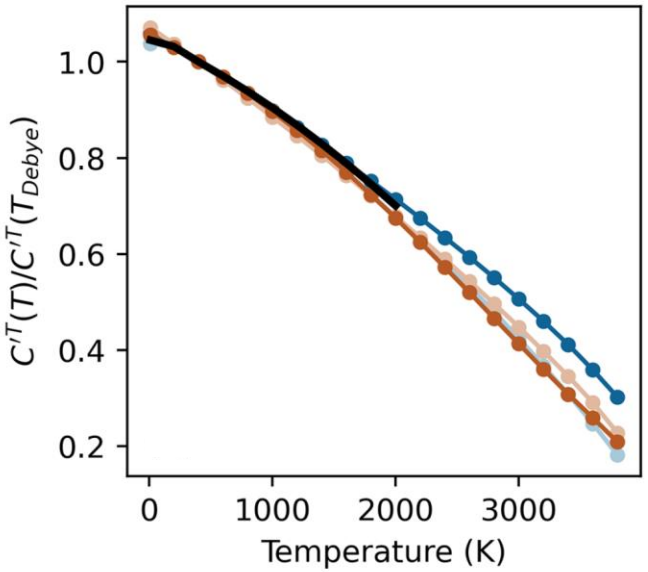

Elastic properties of tungsten are computed using a new algorithm combining the machine learning of the force field at *ab initio* accuracy with a Bayesian sampling scheme aiming at estimating the fully anharmonic free energy.

Elastic constants are evaluated approximately 100 times faster than the existing methods. Calculations predict elastic properties in the temperature range from 2100 K to melting, not accessible to experiment.

Data-driven algorithms for predictive modelling of microstructure

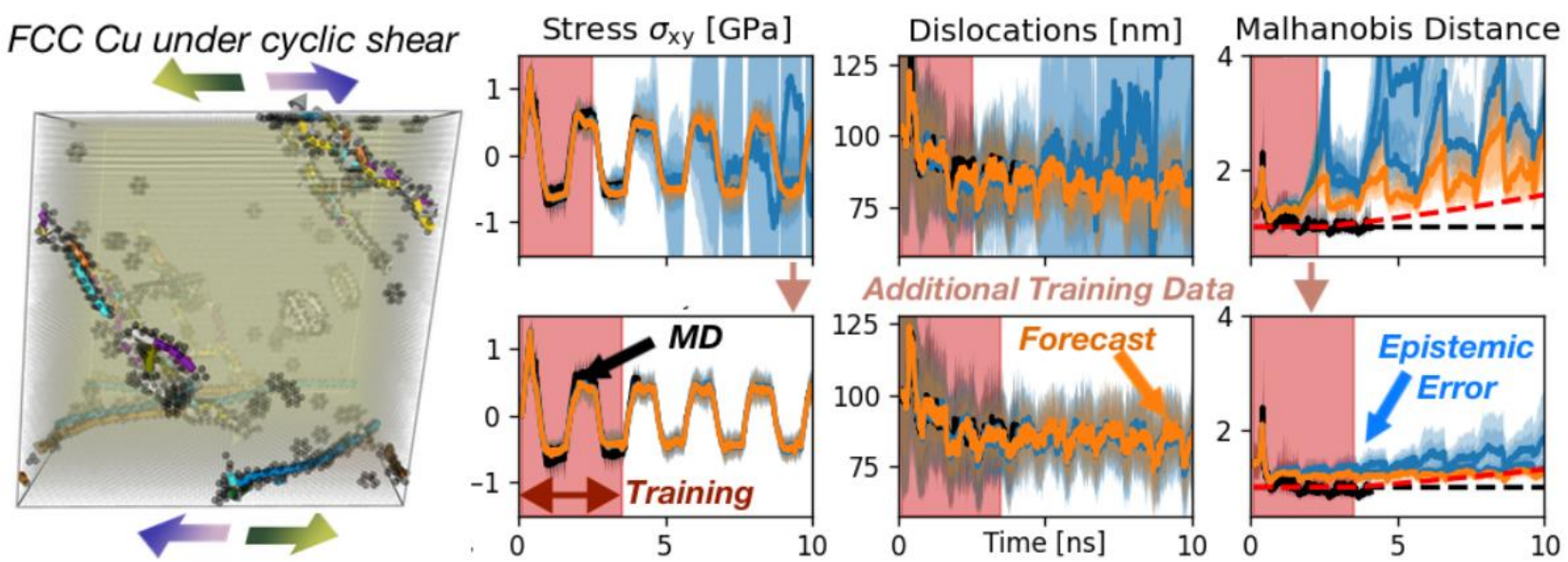

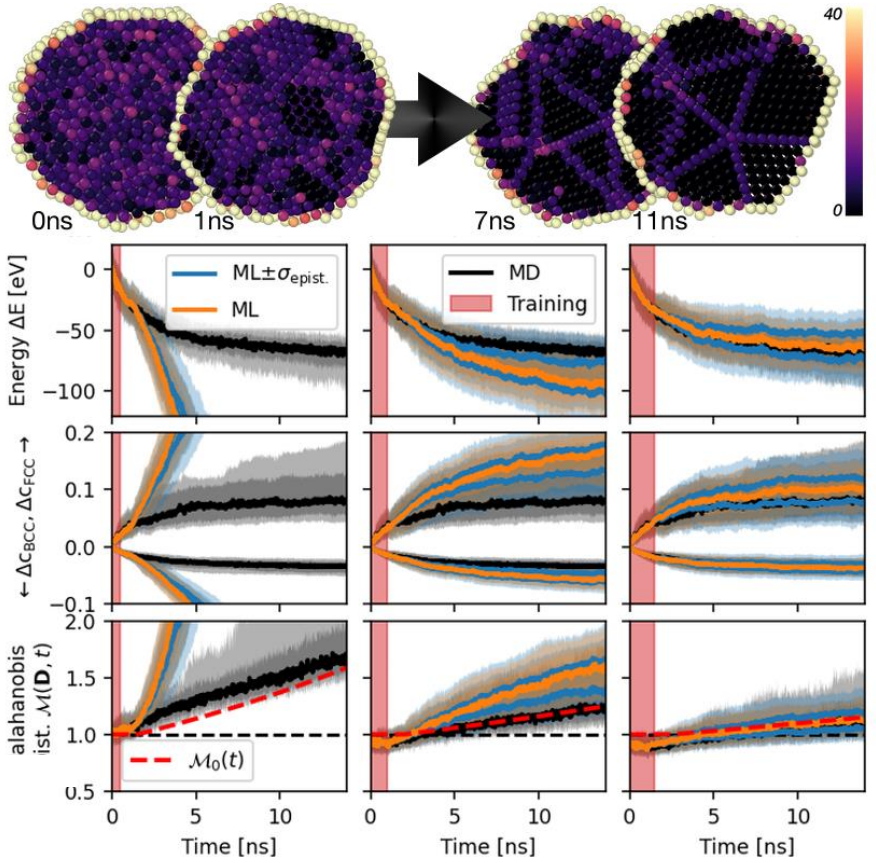

Complexities of material deformation limit the applicability of existing coarse graining and acceleration schemes, which require timescale separation and use low rank (typically 1–4) collective variables. Defining collective variables for extended defects remain elusive, and arbitrary approximations, involving for example the migration of isolated defects are used instead.

A new method mapping atomic positions $\mathbf{X} \in \mathbb{R}^{N\times 3}$ to descriptor functions $\bar{\mathbf{D}} \in \mathbb{R}^{\sim 100}$ enables controlled and highly efficient acceleration of atomistic simulations.

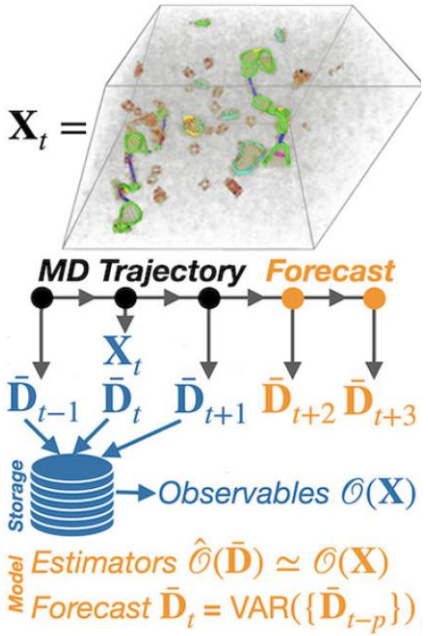

T. D. Swinburne, Phys. Rev. Lett. **131** (2023) 236101

Microstructure is *not* a function of the dose only.

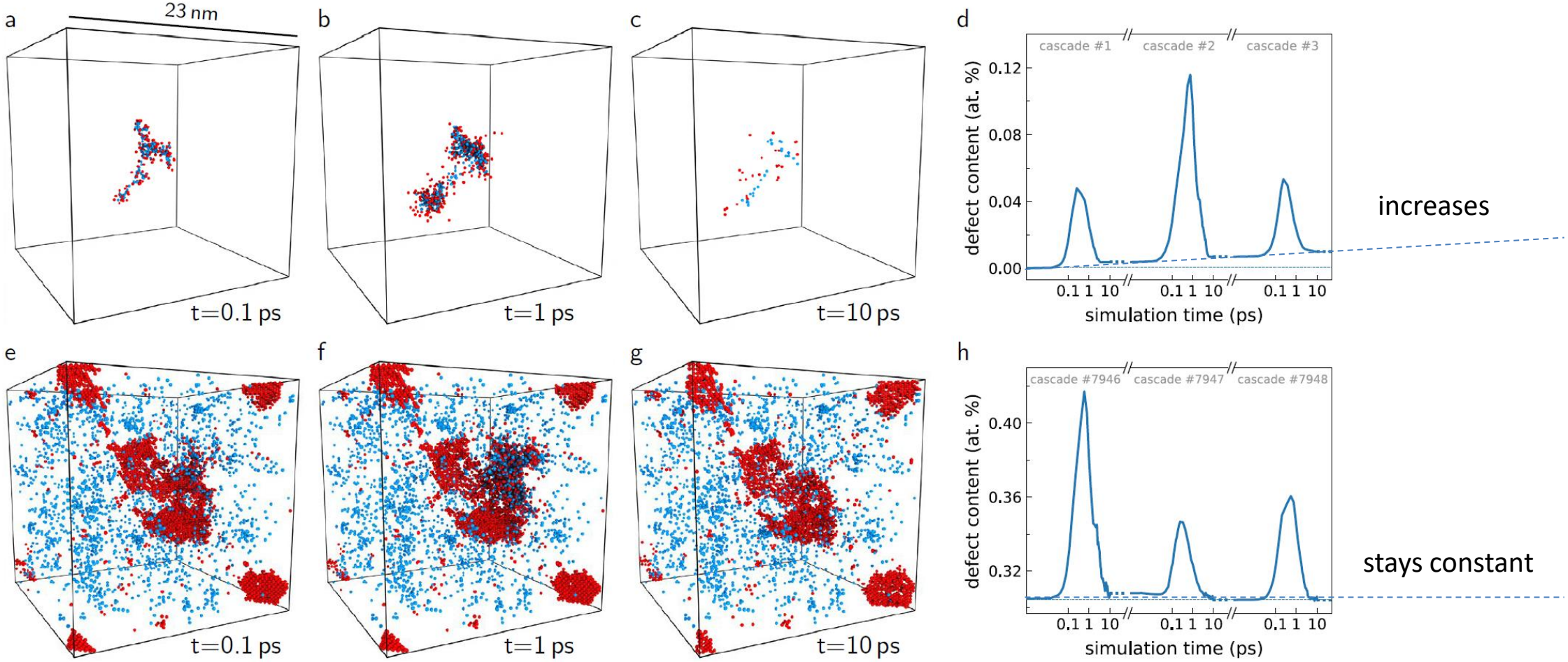

Initially, the defect content increases with each cascade event; BUT in a heavily irradiated material, the defect content fluctuates but remains nearly constant. On average, cascades generate almost no new defects.

M. Boleininger *et al.*, Sci. Reports **13** (2023) 1684

Microstructure is *not* a function of the dose only.

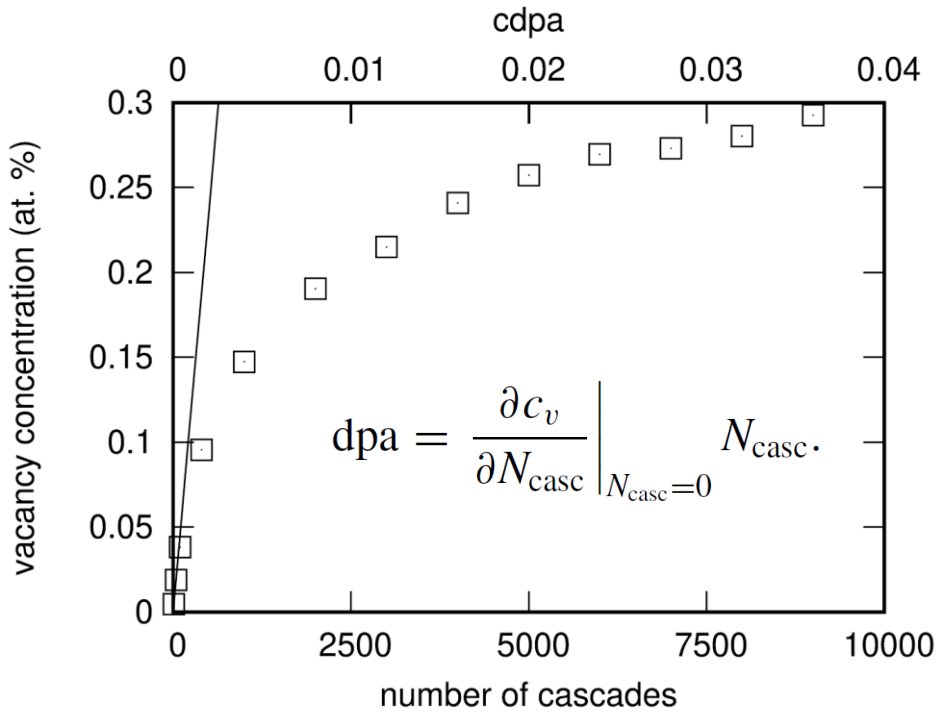

The definition of dpa assumes that the material contains no existing defects; this definition is less useful when applied to a material exposed to a high radiation dose.

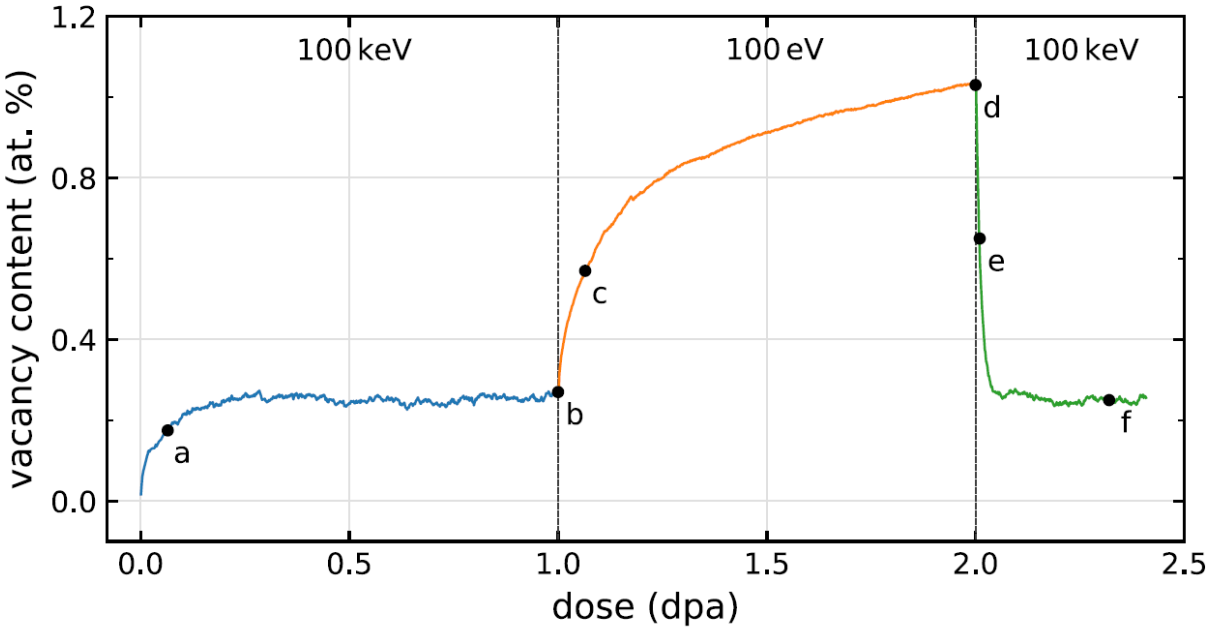

The density of defects in a dynamic steady-state of heavily irradiated material depends on the energy of cascades. Low energy cascades generate more defects at high dose, high energy cascades produce fewer defects at high dose.

"dpa" alone does not characterise the actual physical microstructure; details of recoil spectrum matter.

M. Boleininger *et al.*, Sci. Reports **13** (2023) 1684

Defects as sources of strain and stress

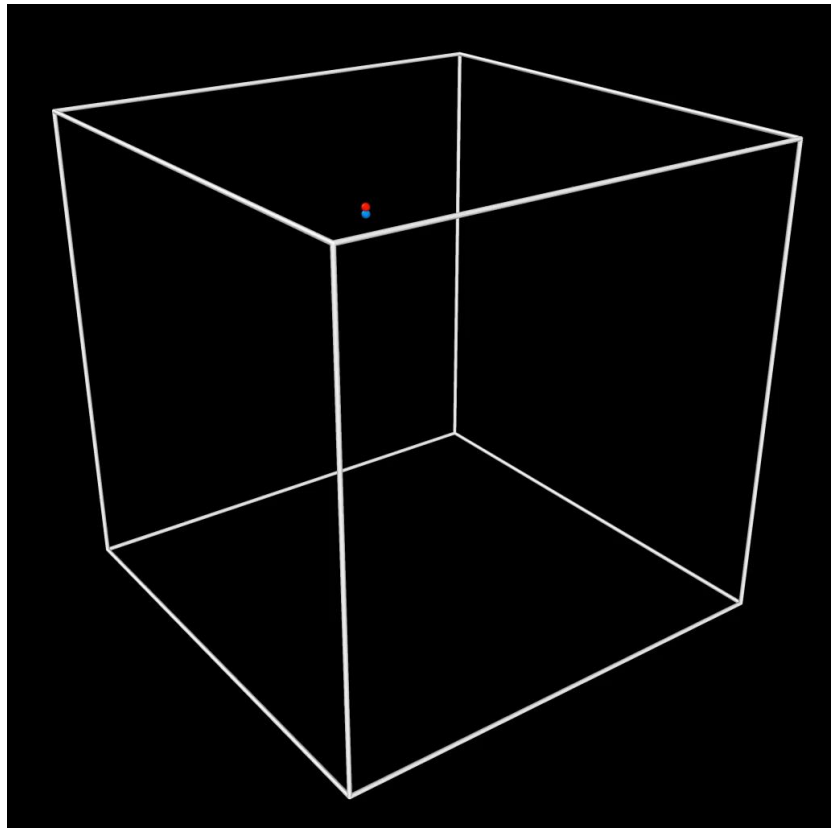

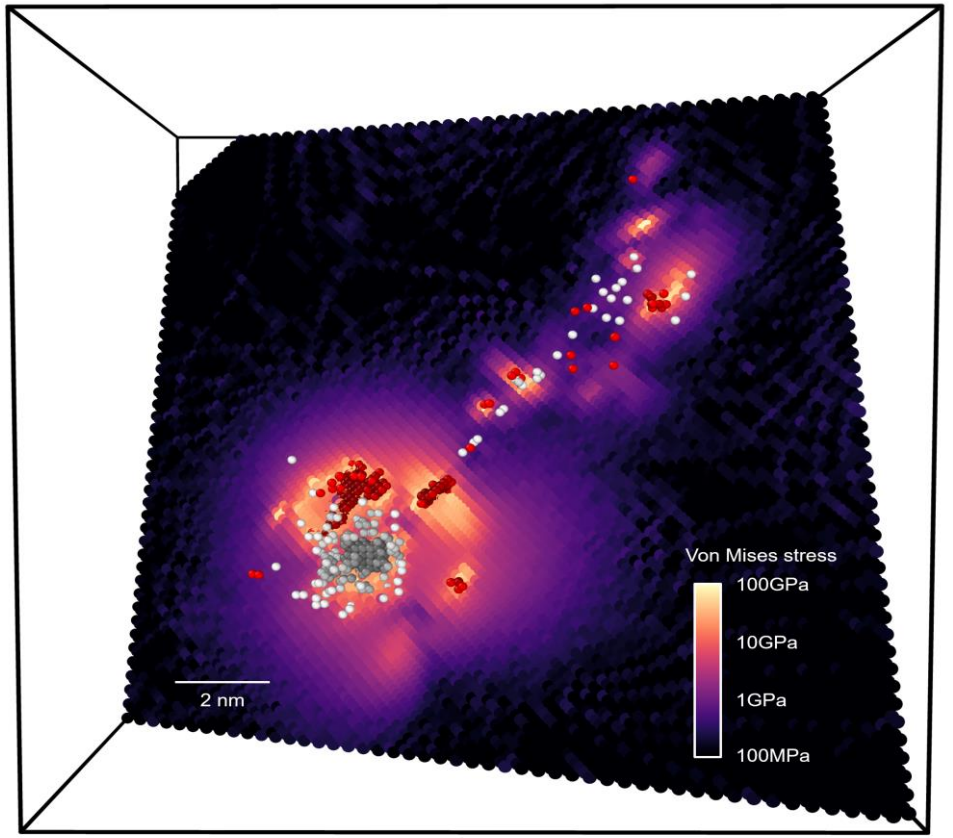

$$\sigma_{von\ Mises} = \sqrt{\frac{3}{2}\left[\mathrm{Tr}(\hat{\sigma})^2 - \frac{1}{3}(\mathrm{Tr}\hat{\sigma})^2\right]}$$

M. Boleininger *et al.*, Sci. Reports **13** (2023) 1684

D.R. Mason *et al.*, J. Appl. Phys. **126** (2019) 075112

Defects as sources of strain and stress

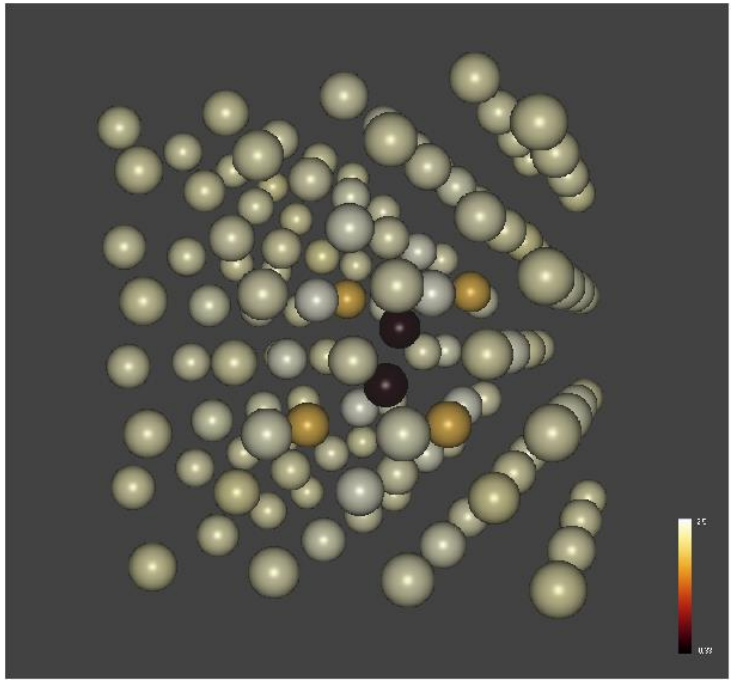

Algorithm for linking microscopic defects to macroscopic continuum deformations:

- dipole tensor of a defect P_{kl}, definition

$$u_i(\mathbf{r}) = -P_{kl}\frac{\partial}{\partial x_l}G_{ik}(\mathbf{r}-\mathbf{R})$$

- relaxation volume tensor is related to the dipole tensor via

$$P_{kl} = C_{klmn}\Omega_{mn}$$

volume tensor

elastic constants

- and the *density* of relaxation volume tensors – a very important step

$$\omega_{mn}(\mathbf{x}) = \sum_a \Omega_{mn}^{(a)}\delta(\mathbf{x}-\mathbf{R}_a) \quad \Longleftrightarrow \quad \rho(\mathbf{r}) = \sum_a q_a\delta(\mathbf{r}-\mathbf{r}_a)$$

Density of relaxation volumes is defined similarly to electric charge density in electrostatics.

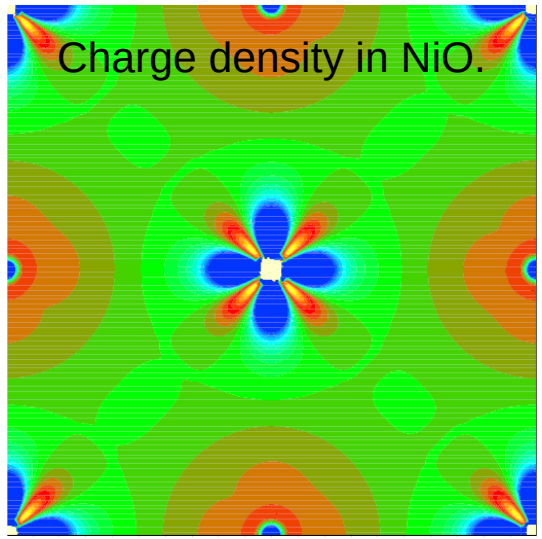

S.L. Dudarev *et al.*, Nuclear Fusion **58** (2018) 126002

Defects as sources of strain and stress: *ab initio* calculations

TABLE XXIV. Elements of the dipole tensor P_{ij} (in eV units), the relaxation volume tensor Ω_{ij} (in Å^3 units), eigenvalues of the relaxation volume tensor $\Omega^{(i)}$ (in Å^3 units), and the relaxation volume of the defect Ω_{rel} (in atomic volume units Ω_0) computed for Fe.

Fe	P_{11}	P_{22}	P_{33}	P_{12}	P_{23}	P_{31}	Ω_{11}	Ω_{22}	Ω_{33}	Ω_{12}	Ω_{23}	Ω_{31}	$\Omega^{(1)}$	$\Omega^{(2)}$	$\Omega^{(3)}$	Ω_{rel}
⟨111⟩d	23.465	23.465	23.472	5.850	5.851	5.851	6.327	6.327	6.335	4.362	4.363	4.363	1.964	1.964	15.051	1.673
⟨111⟩c	23.186	23.186	23.193	5.903	5.904	5.904	6.252	6.252	6.259	4.402	4.402	4.402	1.850	1.850	15.056	1.653
⟨110⟩d	25.832	21.143	21.150	0.000	5.122	0.000	9.777	4.294	4.302	0.000	3.819	0.000	9.777	0.475	8.122	1.620
Tetra	21.396	23.331	23.339	0.000	0.001	0.000	4.607	6.871	6.880	0.000	0.000	0.000	4.607	6.871	6.880	1.619
⟨100⟩d	32.284	22.931	22.937	0.000	0.000	0.000	14.316	3.378	3.385	0.000	0.000	0.000	14.316	3.378	3.385	1.858
Octa	23.273	23.273	31.302	0.000	0.000	0.000	3.869	3.869	13.258	0.000	0.000	0.000	3.869	3.869	13.258	1.851
Vac	−3.081	−3.081	−3.081	0.000	0.000	0.000	−0.831	−0.831	−0.831	0.000	0.000	0.000	−0.831	−0.831	−0.831	−0.220

A 110 SIA defect in bcc Fe expands the crystal by 1.62 atomic volumes.

TABLE XX. Elements of the dipole tensor P_{ij} (in eV units), the relaxation volume tensor Ω_{ij} (in Å^3 units), eigenvalues of the relaxation volume tensor $\Omega^{(i)}$ (in Å^3 units), and the relaxation volume of the defect Ω_{rel} (in atomic volume units Ω_0) computed for W.

W	P_{11}	P_{22}	P_{33}	P_{12}	P_{23}	P_{31}	Ω_{11}	Ω_{22}	Ω_{33}	Ω_{12}	Ω_{23}	Ω_{31}	$\Omega^{(1)}$	$\Omega^{(2)}$	$\Omega^{(3)}$	Ω_{rel}
⟨111⟩d	52.754	52.754	52.754	13.128	13.128	13.128	9.209	9.209	9.209	7.402	7.402	7.402	1.808	1.808	24.012	1.712
⟨111⟩c	52.745	52.745	52.745	13.151	13.151	13.151	9.207	9.207	9.207	7.414	7.414	7.414	1.793	1.793	24.036	1.711
⟨110⟩d	56.960	52.557	52.557	0.000	11.277	0.000	10.908	8.693	8.693	0.000	6.358	0.000	10.908	2.335	15.050	1.753
Tetra	47.359	59.114	59.114	0.000	0.000	0.000	5.693	11.606	11.606	0.000	0.000	0.000	5.693	11.606	11.606	1.791
⟨100⟩d	65.920	53.379	53.379	0.000	0.000	0.000	14.254	7.945	7.945	0.000	0.000	0.000	14.254	7.945	7.945	1.868
Octa	52.741	52.741	67.209	0.000	0.000	0.000	7.623	7.623	14.901	0.000	0.000	0.000	7.623	7.623	14.901	1.868
Vac	−9.984	−9.984	−9.984	0.000	0.000	0.000	−1.743	−1.743	−1.743	0.000	0.000	0.000	−1.743	−1.743	−1.743	−0.324

A vacancy in tungsten contracts the crystal by 0.324 atomic volumes.

P.-W. Ma *et al.*, Phys. Rev. Mat. **3** (2019) 013605;
P.-W. Ma et al., Phys. Rev. Mat. **5** (2021) 013601

Tensor volumes of dislocation loops, voids and gas bubbles

$\mathbf{A} = \frac{1}{2}\oint(\mathbf{r}\times d\mathbf{l})$ is the *vector* area of a dislocation loop

$$\Omega_{rel} = (\mathbf{b}\cdot\mathbf{A}) = \frac{1}{2}\oint \mathbf{b}\cdot(\mathbf{r}\times d\mathbf{l})$$

S. L. Dudarev and P.-W. Ma, Phys. Rev. Mat. **2** (2018) 033602

There is also a formula for the volume of an arbitrary dislocation configuration, including individual dislocation loops, stacking fault tetrahedra, dislocation networks etc.

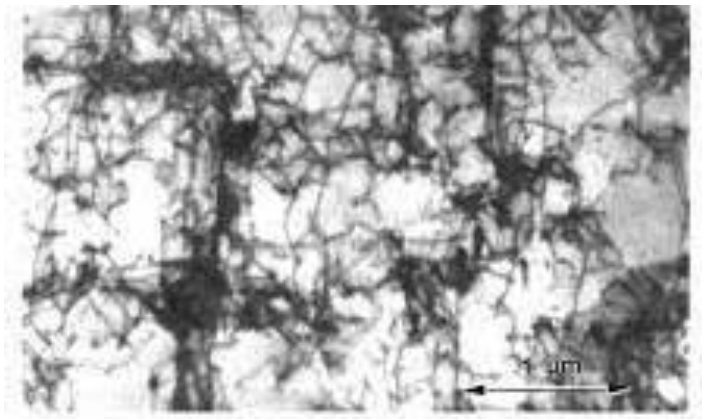

$$\Omega_{ij} = \frac{1}{4}\sum_{(n)}\left(b_i^{(n)}\epsilon_{jkl} + b_j^{(n)}\epsilon_{ikl}\right)\int_{(n)} x_k dx_l$$

M. Boleininger *et al.*, Phys. Rev. Mat. **6** (2022) 063601

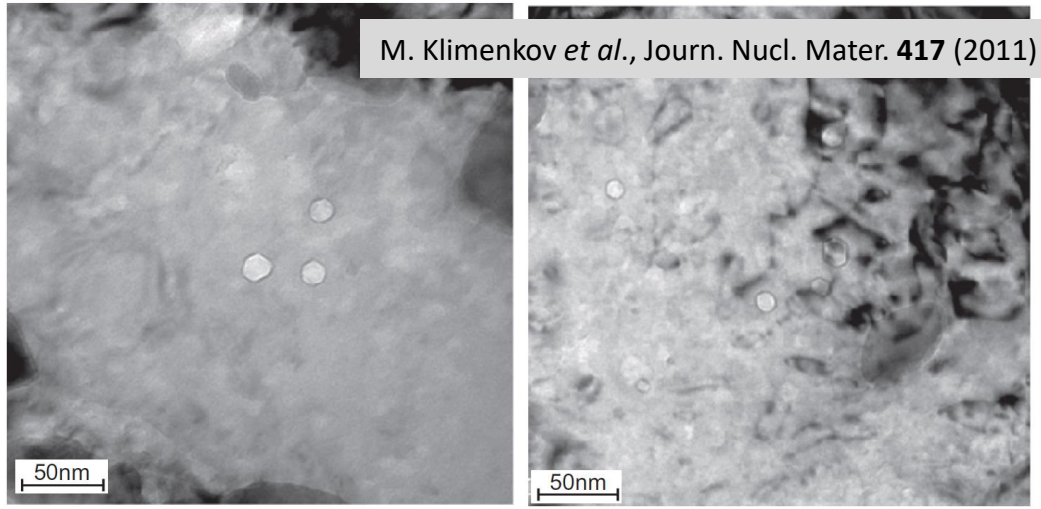

M. Klimenkov *et al.*, Journ. Nucl. Mater. **417** (2011) 124

Fig. 4. Bright field TEM micrographs of He bubbles or voids in EUROFER 97 irradiated at 350 °C.

$$\Omega_{ij} = \frac{\pi a^3}{\mu}\left(\frac{1-\nu}{1+\nu}\right)\left(p_a - \frac{2\gamma}{a}\right)\delta_{ij}$$

The relaxation volume of a gas bubble, *P* is the pressure of gas in the bubble, *γ* is the surface tension, *a* is the radius of the bubble. If *P=0* then:

$$\Omega_{ij} = -2\pi\left(\frac{1-\nu}{1+\nu}\right)\frac{\gamma a^2}{\mu}\delta_{ij}$$

The relaxation volume tensor of a void is isotropic and the volume itself is negative.

D.R. Mason *et al.*, J. Appl. Phys. **126** (2019) 075112

Lattice strain from radiation defects

D.R. Mason *et al.*, Phys. Rev. Lett. **125** (2020) 225503

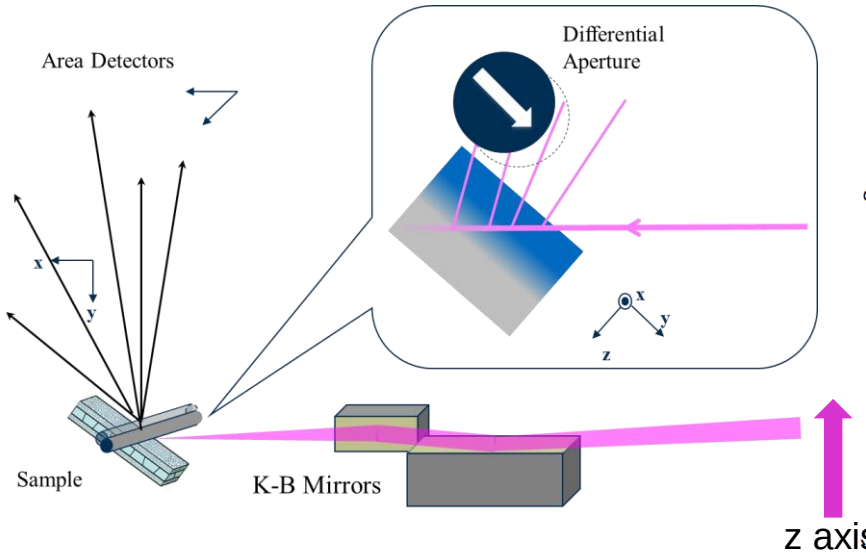

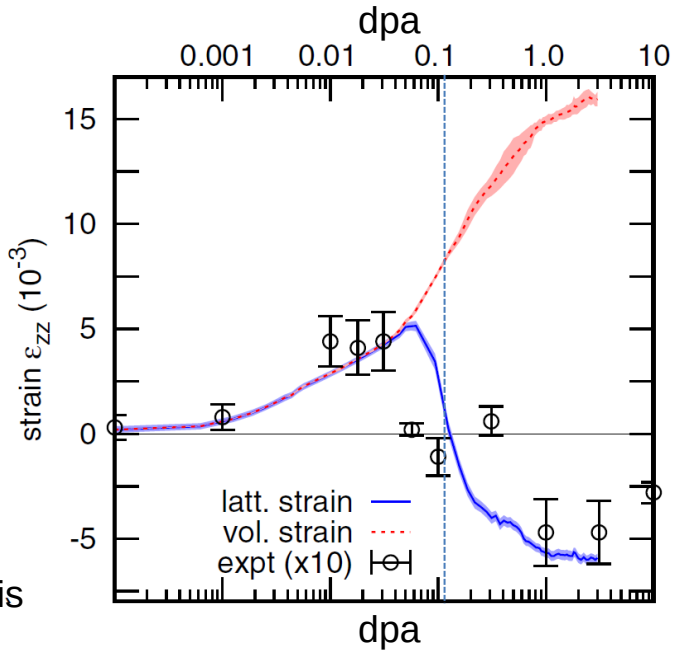

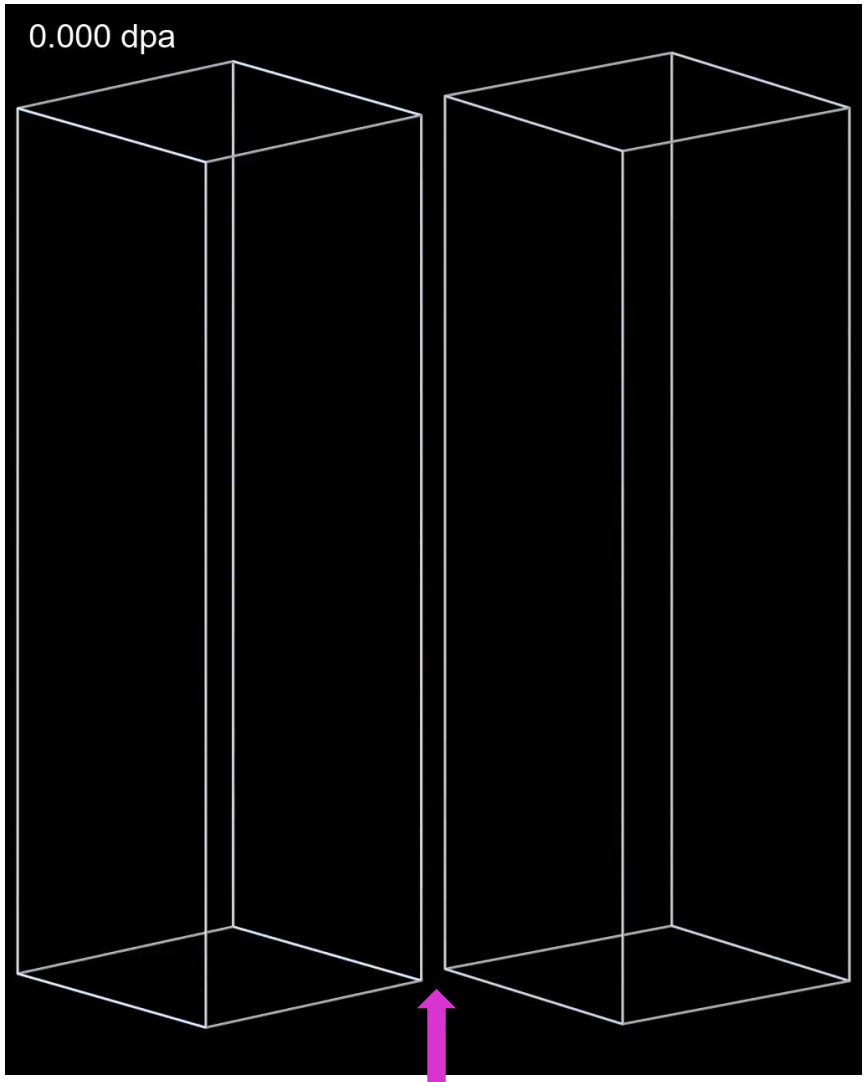

Lattice strain in ion-implanted tungsten, observed using X-ray diffraction and simulated using the creation-relaxation algorithm (CRA) with no adjustable parameters.

Evolution of strain is non-linear and results from the accumulation and coalescence of defects. Transition from positive to negative lattice strain shows that vacancies dominate at high (>0.1 dpa) dose.

M. Boleininger *et al.*, Sci. Reports **13** (2023) 1684

FEM: the role of *gradients* of neutron exposure

If defects are homogeneously distributed, the material expands or contracts; there is no stress. Stress and elastic deformations arise if the density of defects varies across a component, compressive and dilatational stress results from a combined effect of varying swelling and boundary conditions

$$\epsilon_{ij}(\mathbf{x}) = \epsilon_{ij}^{(\mathrm{tot})}(\mathbf{x}) - \omega_{ij}(\mathbf{x})$$

elastic strain

total strain

relaxation volume density of defects, *ditto* eigenstrain

Structural integrity criteria involve elastic strain, which changes sign across a component (Albenga's theorem).

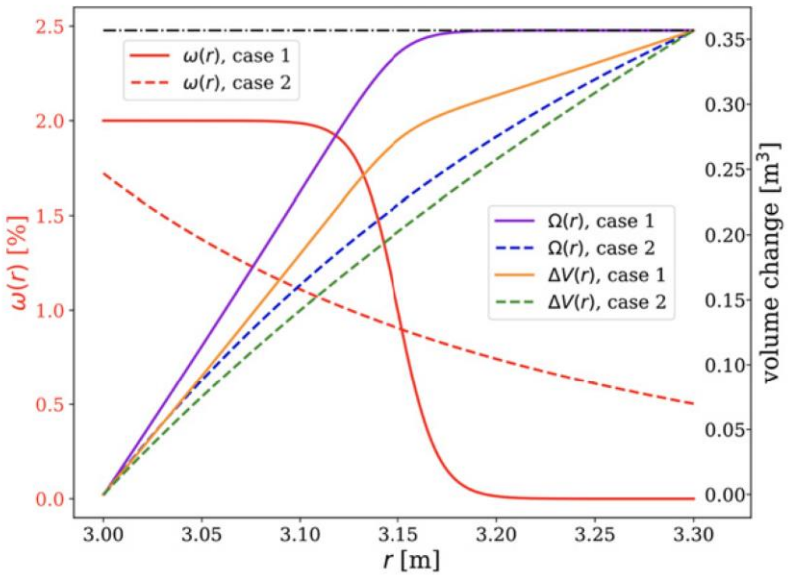

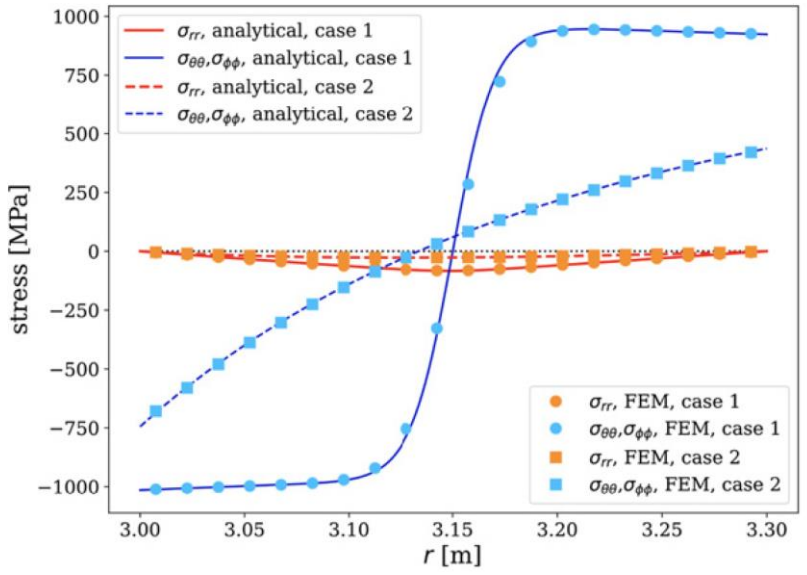

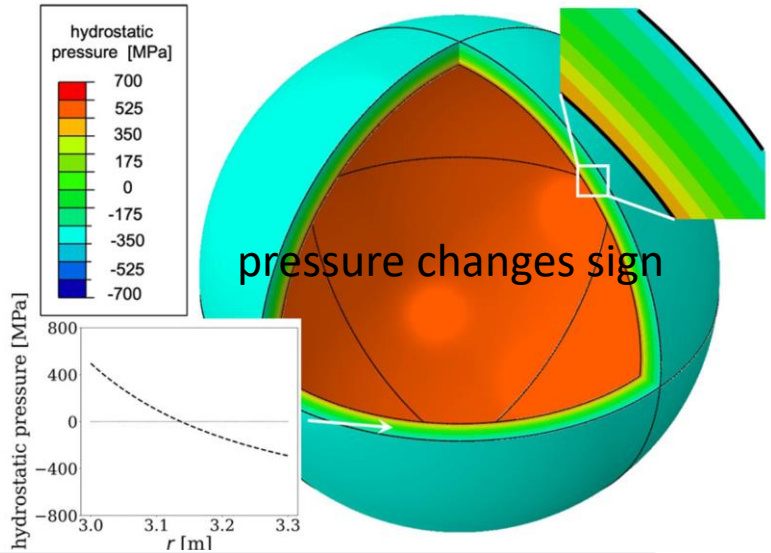

$$p(r) = -\frac{1}{3}\sigma_{ii}(r) = \frac{4\mu}{9}\left(\frac{1+\nu}{1-\nu}\right)[\omega(r) - \overline{\omega}]$$

L. Reali *et al.*, Nuclear Fusion **62** (2022) 016002

FEM: effect of neutron exposure gradients

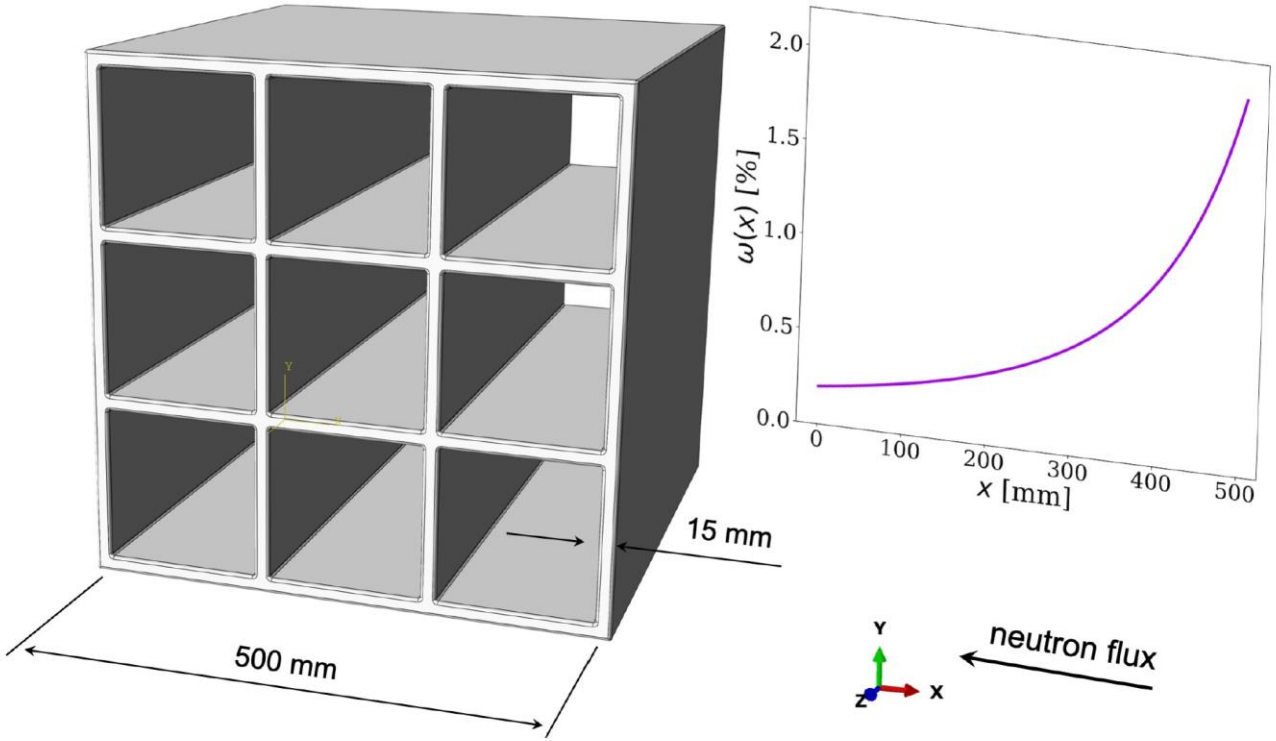

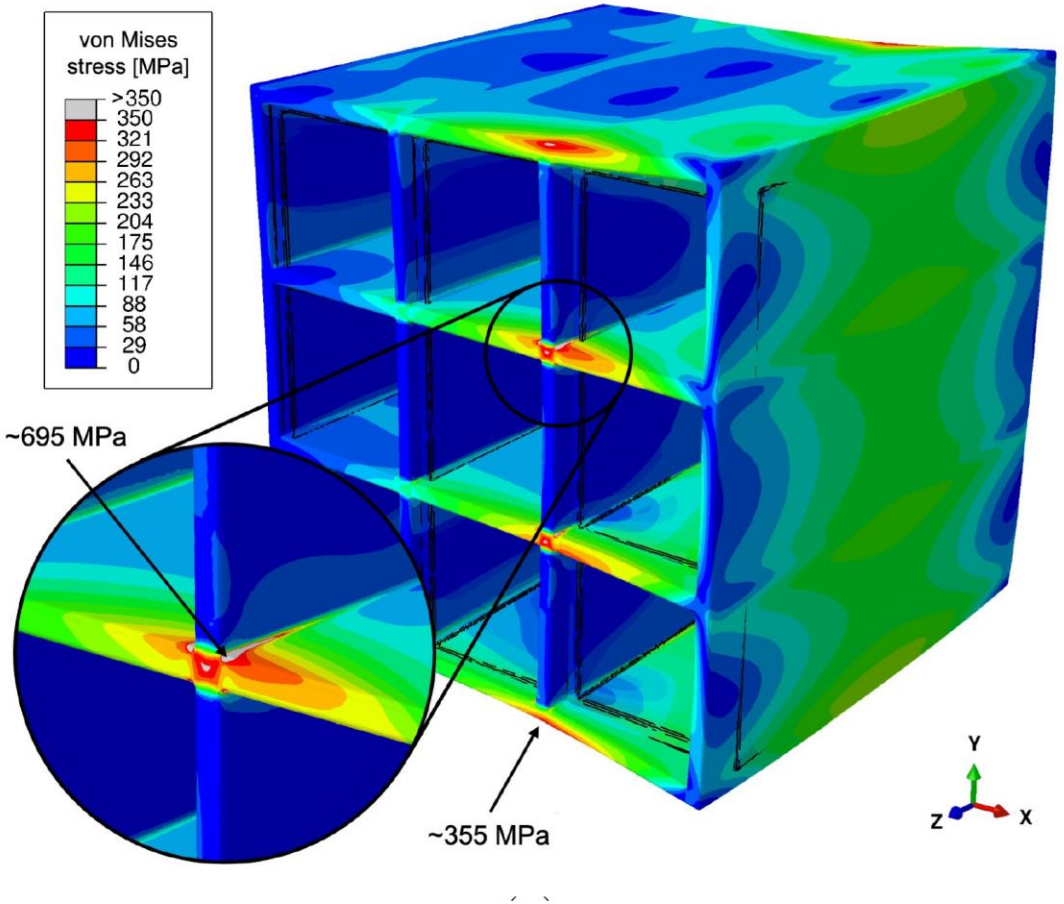

$$\frac{\partial}{\partial x_j}\sigma_{ij}(\mathbf{r}) + \rho g_i - B\alpha(T)\frac{\partial T(\mathbf{r})}{\partial x_i} - B\frac{\partial}{\partial x_i}\omega_{rel}(\mathbf{r}) + f_i^{(magn)}(\mathbf{r}) = 0$$

Unified mechanical equilibrium equation including thermal expansion, gravity, magnetic forces, and radiation effects, treating the defect density gradients as body forces.

L. Reali *et al.*, Nuclear Fusion **62** (2022) 016002; Nuclear Fusion **64** (2024) 056001

FEM: validation of open-source software against commercial codes

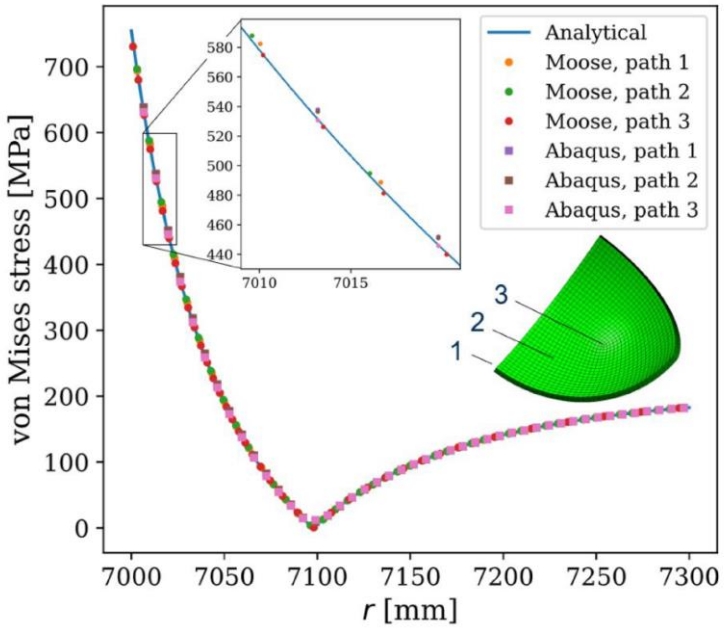

$$\sigma_{\theta\theta}(r) = \sigma_{\phi\phi}(r) = \frac{4\mu}{9}\left(\frac{1+\nu}{1-\nu}\right)\left[\overline{\omega}\left(1+\frac{R_1^3}{2r^3}\right)\right] + \frac{2\mu}{3}\left(\frac{1+\nu}{1-\nu}\right)\left[\frac{1}{r^3}\int_{R_1}^{r} R^2\omega(R)\,\mathrm{d}R\right] - \frac{2\mu}{3}\left(\frac{1+\nu}{1-\nu}\right)\omega(r),$$

$$\sigma_{rr}(r) = \frac{4\mu}{9}\left(\frac{1+\nu}{1-\nu}\right)\left[\overline{\omega}\left(1-\frac{R_1^3}{r^3}\right)\right] - \frac{4\mu}{9}\left(\frac{1+\nu}{1-\nu}\right)\left[\frac{3}{r^3}\int_{R_1}^{r} R^2\omega(R)\,\mathrm{d}R\right].$$

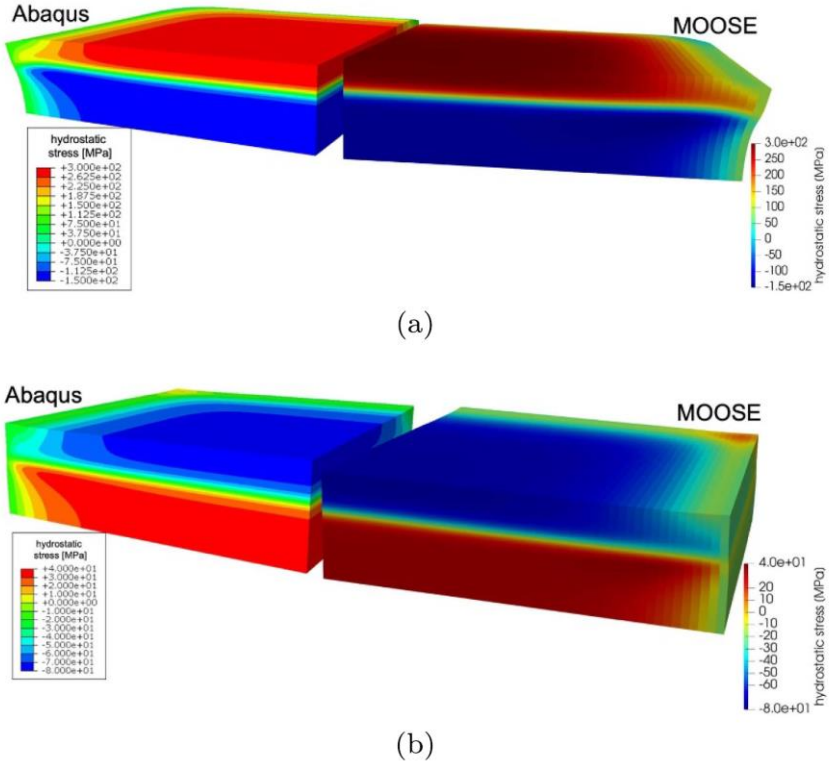

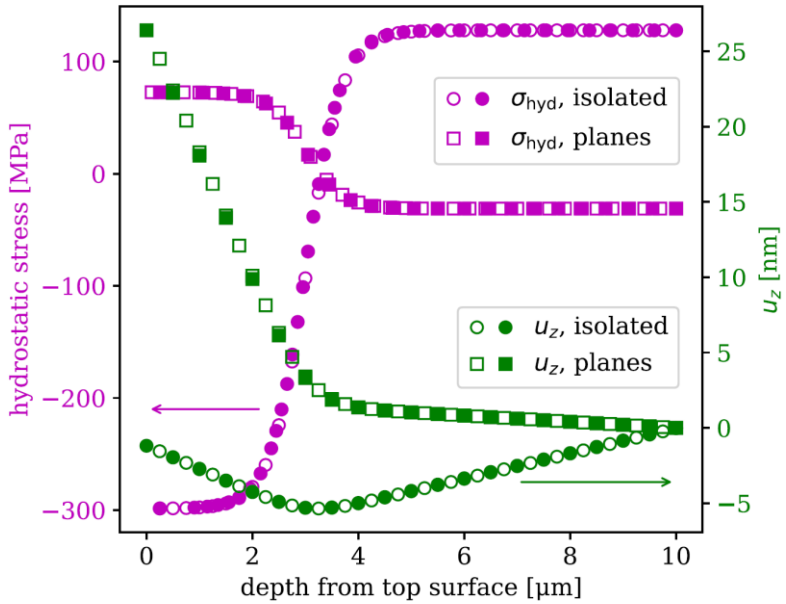

Hollow symbols Abaqus;
filled symbols MOOSE

Demonstrating the feasibility of FEM simulations is only a part of the treatment, matching the potential needs of engineering design.

Large-scale open-source codes for 100M element FEM simulations require validation and benchmarking.

L. Reali and S.L. Dudarev, Nuclear Fusion **64** (2024) 056001

From components to a full tokamak device

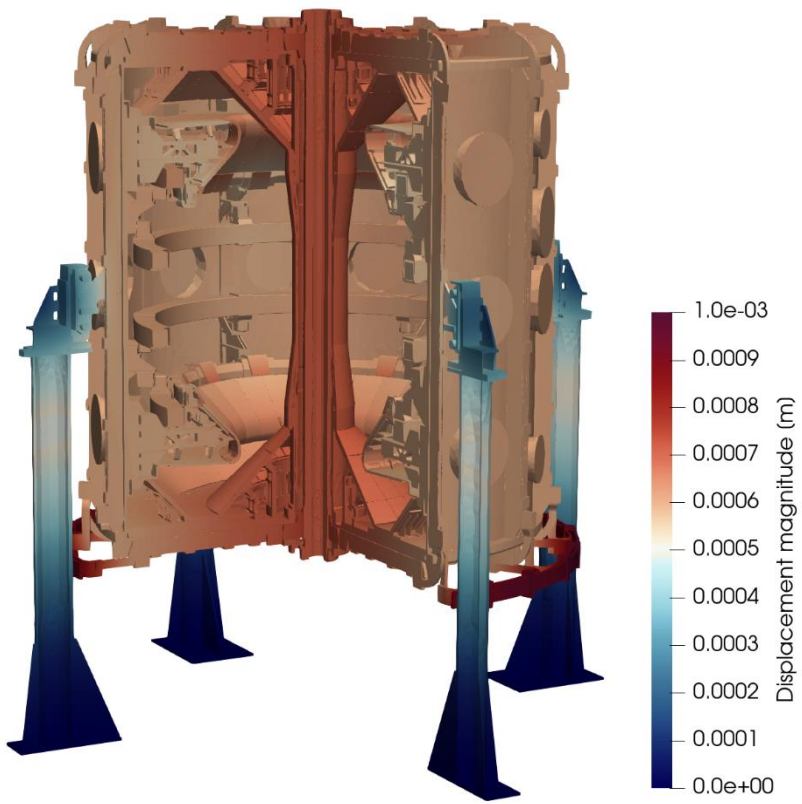

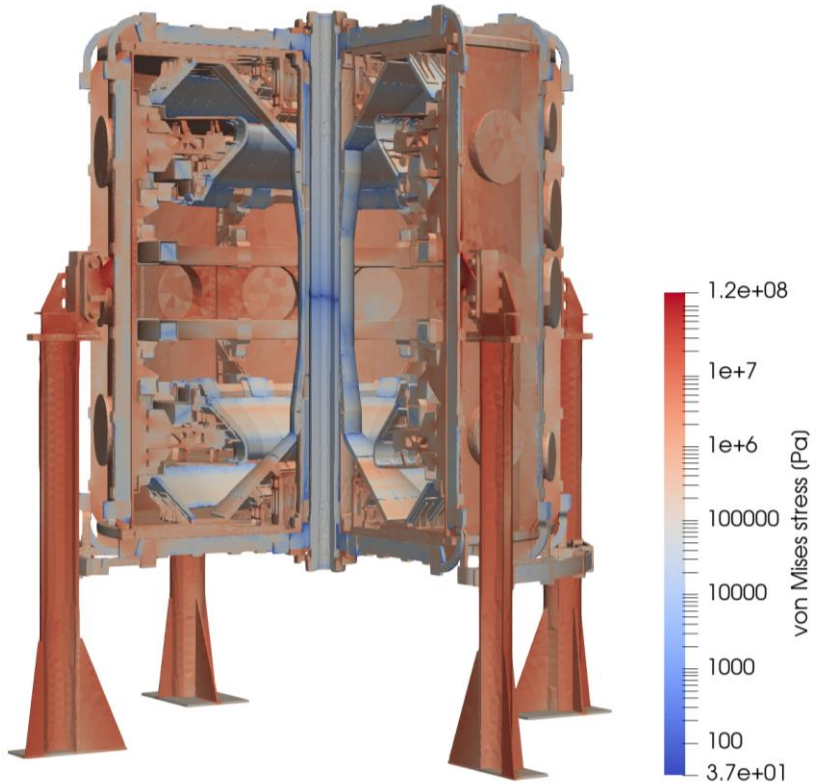

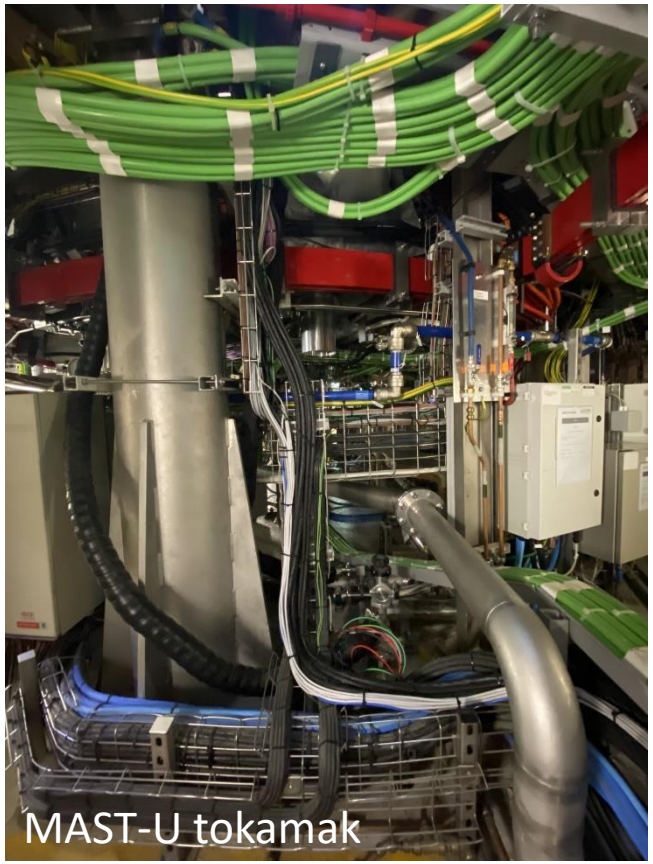

A ~70M finite element model for the MAST-U tokamak, showing gravitational displacements and stress. This application illustrates new concepts and algorithms, linking microscopic and macroscopic scales. This should enable estimating effects of local radiation exposure, magnetic fields, gravitational stress, and temperature on materials in a full reactor prior to its construction.

W.M.E. Ellis, L. Reali, H.M. Brooks, A. Davis, S.L. Dudarev (2024)